THE ASTROPHYSICAL JOURNAL, 314:439–456, 1987 March 15

THE SHAPE OF THE DARK HALO IN POLAR-RING GALAXIES

BRADLEY C. WHITMORE[1]
Space Telescope Science Institute, Baltimore
DOUGLAS B. MCELROY[1,2]
Astronomy Programs, Computer Sciences Corporation
AND
FRANÇOIS SCHWEIZER[1]
Department of Terrestrial Magnetism, Carnegie Institution of Washington
Received 1986 May 15; accepted 1986 September 2

ABSTRACT

Photometric and kinematic observations of the polar-ring galaxies NGC 4650A and ESO 415-G26 (= MCG-05-07-001 = AM 0226-3206) are presented. The inner component of each system is an S0 galaxy, as was previously found in the case of A0136-0801. The existence of polar rings in these galaxies makes it possible to directly measure the gravitational potential of the S0 disk far above and below the plane. A comparison of the circular velocity in the S0 component with the rotation velocity in the polar ring indicates that the halo of dark matter is nearly spherical; the mean value of $V_{\rm ring}/V_{\rm disk}$ for these three galaxies is 0.97 ± 0.08. Estimates for the flattening of equipotentials in the three galaxies are $c/a = 0.86 \pm 0.21$, 1.05 ± 0.17, and 0.98 ± 0.20. These estimates are based on a model with a scale-free potential and are valid for a distance of $\sim 0.6 R_{25}$ from the center.

CCD images of both NGC 4650A and ESO 415-G26 show faint disordered nebulosity in the outer regions, suggestive of tidal debris. This material provides further evidence that the polar rings in these systems resulted from a "second event," which may have been a merger of two galaxies or a near collision with resultant mass transfer. An attempt to age date these events suggests that the polar rings of NGC 4650A and ESO 415-G26 formed most recently (~ 1–3×10^9 yr ago), whereas the polar ring of A0136-0801 probably formed significantly longer ago, with a lower limit of at least 2–3×10^9 yr.

Profiles of rotational velocity and velocity dispersion for the standard galaxies NGC 488, NGC 628, NGC 1052, and NGC 7619 are presented.

Subject headings: galaxies: evolution — galaxies: individual — galaxies: internal motions — galaxies: photometry — galaxies: structure

I. INTRODUCTION

The nature and distribution of dark matter in the universe is one of the central problems of contemporary astronomy. On galactic scales, the existence of significant amounts of dark matter is indicated by observations of rotational velocities in the disks of spiral galaxies (e.g., Rubin, Ford, and Thonnard 1980). However, this technique does not distinguish between a disk-shaped and a spheroidal distribution of the dark matter. The discovery of S0 galaxies with polar rings (NGC 2685: Ulrich 1975; Schechter and Gunn 1978; A0136-0801: Schweizer, Whitmore, and Rubin 1983, hereafter SWR; NGC 4650A: Sérsic 1967; Laustsen and West 1980; Schechter, Ulrich, and Boksenberg 1984) provides an unexpected but welcome method of determining the shape of the gravitational potential. This technique was first used by SWR. A comparison of the circular velocities in the S0 disk with the rotational velocities in the polar ring of A0136-0801 suggested that the dark halo of this system is more nearly spherical than disk-shaped.

The existence of two components rotating at nearly right angles would be difficult to understand in terms of the collapse of a single protogalactic cloud. A "second event" in the formation history of these galaxies seems indicated. This event might be the merging of a gas-rich companion with an S0 galaxy, or the transfer of mass from a companion galaxy. In SWR we suggested that the stellar material would disperse into the halo, while the gaseous material would suffer dissipation and would quickly settle into a new disk. If this gaseous disk is nearly orthogonal to the inner S0 disk, the lifetime against disruption by differential precession would be quite long.

Previous studies of polar-ring galaxies centered on the problem of determining their basic geometry. Is the central galaxy a prolate "spindle"-shaped elliptical, or is it a normal S0 disk seen edge-on? The resulting observations clearly showed the latter to be the case. The most convincing piece of evidence was that the ratio of rotational velocity to velocity dispersion V/σ is always larger than ~ 1.0 for the inner component, indicating that it is a rotationally supported disk.

Once the geometry of these galaxies was understood, several new questions arose (see review by Athanassoula and Bosma 1985): how common are polar-ring galaxies, why are some rings narrow while others are more disklike, are polar rings found in isolated environments or clusters? Perhaps the most important problem is a determination of the age of these systems. Are the polar rings quasi-stable, with a settling time determined by differential precession (Tohline, Simonson, and Caldwell 1982), or are they equilibrium configurations,

[1] Visiting Astronomer, Cerro Tololo Inter-American Observatory, National Optical Astronomical Observatories, which is operated by the Association of Universities for Research in Astronomy, Inc., under contract with the National Science Foundation.
[2] Staff Member, Space Telescope Science Institute.

perhaps stabilized by triaxiality of the S0 disk (Steiman-Cameron and Durisen 1982; Lake and Norman 1983) or of the dark halo (SWR; Whitmore 1984)? The determination of age is important both for a theoretical understanding of how these, and more normal, systems formed, and because it would make it possible to determine the frequency of accretion events.

The primary goal of this paper is to present observations of NGC 4650A and ESO 415-G26 (= MCG-05-07-001 = AM 0226-3206) which are similar in quality to the observations of A0136-0801 reported in SWR (§§ II and III). We then address the two main questions outlined above: what is the shape of the gravitational potential, and what can be determined about the age and stability of these systems (§ IV)? We also make a guess about the formation history of the above-mentioned three systems. Our conclusions are summarized in § V. Finally, the Appendix gives detailed stellar velocities and velocity dispersions of four standard galaxies used to test the reliability of our measuring technique.

II. OBSERVATIONS AND REDUCTIONS

An observing log is provided in Table 1. Photometric observations were made using the prime focus CCD on the 4 m telescope at Cerro Tololo Inter-American Observatory. These observations were used to test whether the luminosity profile of the inner component is that of a disk or of an elliptical galaxy, to determine mass-to-light ratios, to study the stellar content of the ring by measuring $B-V$ colors, and to search for faint material in the outer regions which would be indicative of a recent accretion. Spectroscopic observations were obtained with the 4 m Ritchey-Chrétien spectrograph plus the Carnegie two-stage image tube to determine the kinematics of both the gaseous and stellar components. From the kinematics, we determine the mass and mass-to-light ratios of the galaxies and the flattening of their gravitational potential.

a) Photometric Observations

A blue image of NGC 4650A was kindly supplied by Dr. Nelson Caldwell. Since it lacked calibration, a value of $B_{sky} = 22.28 \pm 0.3$ mag arcsec^{-2} obtained from our 1984 November observations was used to determine the magnitude zero point. The Moon was down during both sets of observations. The uncertainty estimate comes from the fact that the CTIO Users Manual quotes a typical value of $B_{sky} = 22.0$, while SWR used 22.55 based on previous observations at CTIO. A V image of NGC 4650A is not available.

The spatial scale of the detector was $0''.582 \pm 0''.004$ pixel^{-1}, and the seeing was generally $\sim 1''.6$ (full width at half-maximum) for both the NGC 4650A and ESO 415-G26 images. Seven standard stars from two different regions observed by Graham (1982) were used to calibrate the 1984 November data; the scatter in the zero point determination was 0.04 mag. We used mean extinction coefficients for CTIO: $K_V = 0.17$ mag and $K_B = 0.27$ mag (Graham 1982). The latter value assumes $B-V = 0.8$ for all objects. The color term is sufficiently small that a difference in $B-V$ of 0.3 mag results in an error in K_B of only 0.004 mag.

The background sky brightness is removed by subtracting a plane which is fitted to ten blank regions around the galaxy. In addition to the B_{sky} level cited above, we obtained an average V_{sky} value of 21.34 mag arcsec^{-2}. Uncertainties in our fit to the sky are $\sim 0.5\%$ of the sky brightnesses, corresponding to uncertainties of 0.15 mag arcsec^{-2} at our last data point ($B \approx 26$ mag arcsec^{-2} and $V \approx 25$ mag arcsec^{-2}).

To check our photometry, we also observed NGC 2775 for comparison with Boroson (1981). Figure 1 shows the comparison in B. The agreement in the range 4″–45″ is good, with an average residual of 0.03 ± 0.08 mag. Boroson's magnitudes in the inner 4″ are systematically high by up to 0.4 mag, as previously found by Whitmore and Kirshner (1982). The error in

TABLE 1

OBSERVING LOG

Object	Exposure Time (minutes)	Position Angle	Wavelength Range (Å)	Resolution (FWHM in Å)	Date
Photometry: Prime Focus CCD, 4 m Telescope at CTIO					
NGC 4650A[a]	17	...	B	...	1984 Mar 11
ESO 415-G26	42	...	B	...	1984 Nov 18
	20	...	V	...	1984 Nov 18
Spectroscopy:[b] Ritchey-Chrétien Spectrograph + Carnegie Image Tube, 4 m Telescope at CTIO					
Program galaxies:					
NGC 4650A	90	63°	3700–5500	3.5	1983 Aug 10
	120	158	6250–7200	0.9	1983 Jun 13
ESO 415-G26	110	16	3700–5500	3.5	1984 Nov 16
	30	92	3700–5500	3.5	1984 Nov 16
	113	92	6250–7200	3.5	1984 Nov 17
Standard galaxies (for comparison):					
NGC 488	60	8	3700–5500	3.5	1983 Aug 10
NGC 628	15	90	3700–5500	3.5	1984 Nov 17
NGC 1052	10	120	3700–5500	3.5	1984 Nov 17
NGC 7619	15	30	3700–5500	3.5	1983 Aug 10

NOTE.—Several fields of photometric standard stars were observed to calibrate the magnitude scale. Several stars were also observed during each observing run to be used in the Fourier quotient reductions as template spectra. These ranged in type from F2 III to K2 III.

[a] Frame courtesy of Nelson Caldwell.

[b] Slit width 1″.6 for spectra with 3700–5500 Å range; 1″.3 for spectra with 6250–7200 Å range.

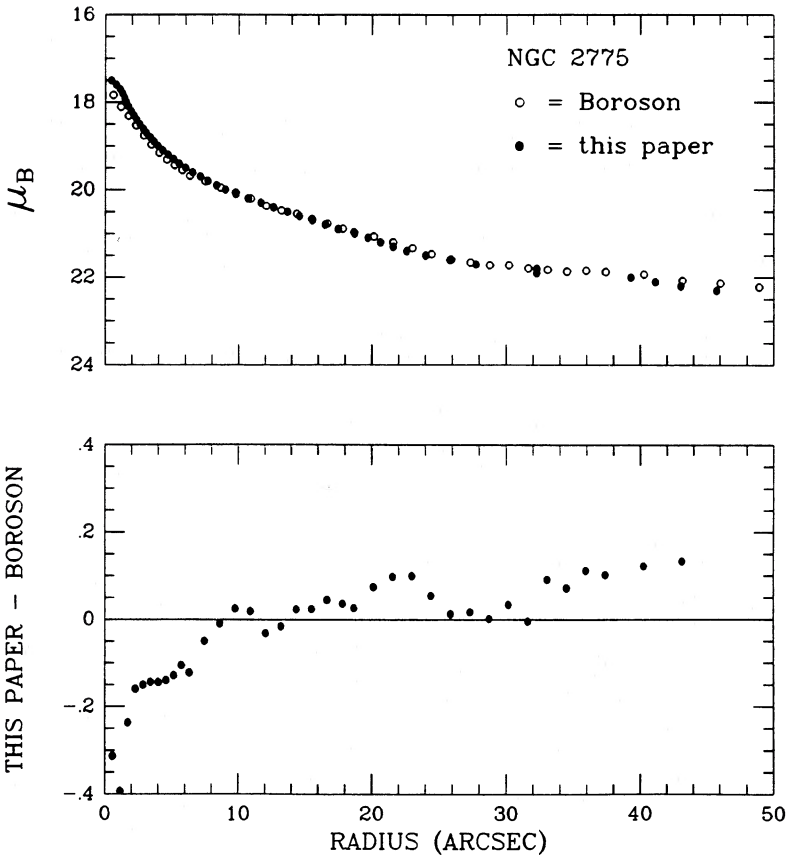

FIG. 1.—Comparison of the brightness profiles of NGC 2775 measured in this paper with observations by Boroson (1981)

Boroson's algorithm for performing the elliptical averaging (discussed by Whitmore and Kirshner) is not important for this comparison, since NGC 2775 is seen nearly face-on.

The resulting brightness profiles along the major axes of the S0 disks and the polar rings are given in Table 2 and shown in Figure 2 and Figure 6 below. Negative radii refer to points east of a north-south line through the nucleus. Figure 3 (Plate 12) shows six different images of NGC 4650A at different contrast levels.

b) *Rotation of the Polar-Ring Gas*

Spectra centered on Hα were taken with the slit of the spectrograph aligned along the major axes of the polar rings. These spectra were measured at DTM using a Mann two-screw measuring engine. Night-sky lines were used to determine the wavelength scale. The resulting heliocentric radial velocities and rotational velocities are listed in Table 3 and shown in Figures 2 and 6. Rotational velocities were calculated from the heliocentric velocities through the relation

$$V = \frac{cz - V_0}{\sin i(1 + z)}, \qquad (1)$$

where V_0 is the systemic value of cz, i is the inclination of the ring, and $(1 + z)$ is the relativistic correction. An additional 10% correction was made to the velocities of NGC 4650A to correct for the fact that the warp of the polar ring makes it impossible to align the slit with the major axis at every point. This is discussed more fully in § III*a*.

The integrated mass within a radius R was calculated through the relation

$$M(R) = 2.3265 \times 10^5 V^2 R, \qquad (2)$$

where V is the rotational velocity in km s^{-1}, R is the radius in kpc, $M(R)$ is the mass interior to R in solar masses, and the numerical constant is the inverse gravitational constant G^{-1} expressed in convenient astronomical units. Equation (2) assumes circular orbits and a spherical gravitational potential.

c) *Stellar Velocities in the* S0 *Disk*

The rotational velocity and velocity dispersion of the stellar components were measured from absorption-line spectra covering the range from 3700 Å to 5500 Å. Only the range from 4100 Å to 4540 Å was used for the measurements. The spectra were scanned with the PDS microdensitometer of the Goddard Space Flight Center using a 16 × 16 μm aperture stepped at 16 μm intervals in wavelength (0.75 Å) and position (0″.38). Spectral scan lines were later co-added in groups of four to produce spectra separated by 1″.5. Reductions were similar to those described in SWR, but with each channel now corresponding to 30 km s^{-1}. The Fourier quotient technique developed by P. Schechter (Sargent *et al.* 1977) was used to determine the rotational velocity, velocity dispersion, and line strength index. Several stars used as templates in the reductions were observed with the same instrumental setup. Generally, a G8 III or K1 III star provided the best fit. Rotational velocities were calculated using equation (1). A correction for line-of-sight integration was included when appropriate (see § IV*a*). Numerical experiments indicated that

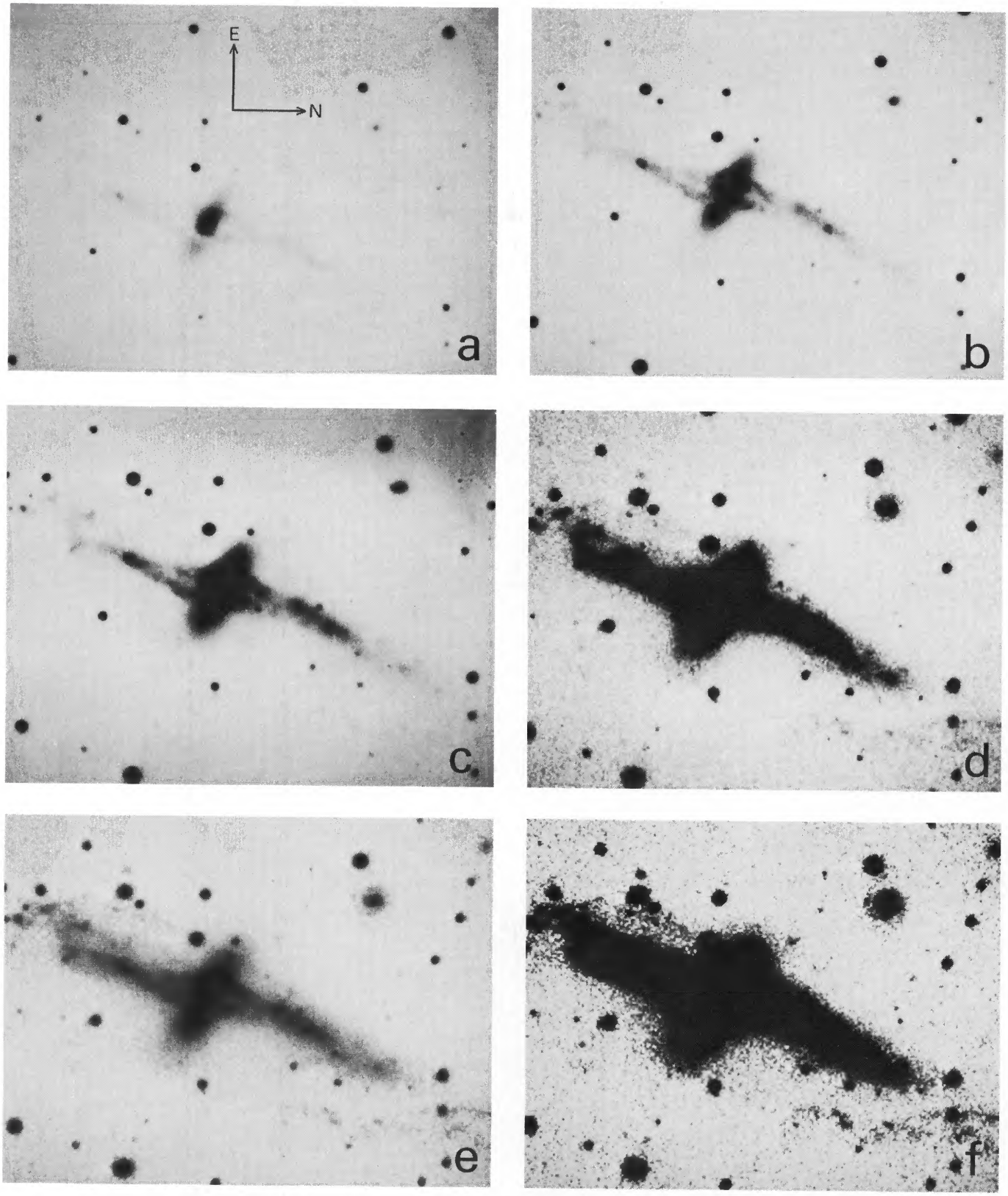

FIG. 3.—Blue image of NGC 4650A displayed at six different contrasts. All the displays are on a linear gray scale, except (*e*) uses a logarithmic gray scale.

WHITMORE, MCELROY, AND SCHWEIZER (*see* page 441)

TABLE 2

LUMINOSITY PROFILES FOR NGC 4650A AND ESO 415-G26

NGC 4650A			ESO 415-G26				NGC 4650A			ESO 415-G26			
R (″)	PA = 61° (B)	PA = 161° (B)	PA = 18° (B)	PA = 18° (V)	PA = 94° (B)	PA = 94° (V)	R (″)	PA = 61° (B)	PA = 161° (B)	PA = 18° (B)	PA = 18° (V)	PA = 94° (B)	PA = 94° (V)
	NE	SE	NE	NE	E	E	0.6	18.61	18.60	18.90	17.64	18.96	17.66
-61.4	—	24.49	—	—	—	—	1.2	19.41	19.24	19.08	18.00	19.33	18.24
-57.0	—	24.54	—	—	—	—	1.7	19.86	20.07	19.43	18.47	19.87	18.91
-54.1	—	25.31	—	—	—	—	2.3	10.39	20.51	19.83	18.94	20.43	19.56
-51.2	—	25.41	—	—	—	—	2.9	20.81	20.94	20.18	19.30	20.97	20.15
-48.3	—	24.99	—	—	—	—	3.5	21.30	21.36	20.55	19.63	21.48	20.68
-45.4	—	24.29	—	—	—	—	4.1	21.64	21.61	20.92	19.96	21.92	21.13
-42.5	—	23.48	25.95	25.27	—	—	4.7	21.70	21.80	21.16	20.16	22.31	21.52
-39.6	—	23.40	25.69	24.85	—	—	5.2	21.55	21.93	21.36	20.35	22.63	21.84
-36.7	—	23.33	25.61	24.59	—	—	5.8	21.37	21.98	21.55	20.53	22.95	22.16
-34.3	—	23.02	25.52	24.40	—	—	6.4	21.28	22.02	21.75	20.74	23.19	22.39
-32.6	—	22.96	25.19	24.32	—	—	7.0	21.24	21.96	21.89	20.88	23.36	22.60
-30.8	—	22.82	25.05	24.00	26.06	24.93	7.6	21.26	21.99	21.94	20.92	23.52	22.76
-29.1	—	22.75	24.86	23.88	25.69	24.86	8.1	21.32	22.08	21.95	20.90	23.75	22.92
-27.4	—	21.96	24.71	23.73	25.32	24.61	8.7	21.36	22.23	21.91	20.87	23.95	23.08
-25.6	25.59	21.78	24.40	23.52	25.09	24.39	9.3	21.46	22.35	21.89	20.88	24.00	23.12
-23.9	25.33	22.33	24.13	23.17	—	—	9.9	21.57	22.30	21.89	20.92	24.09	23.23
-22.4	24.80	22.36	23.88	22.94	—	—	10.5	21.70	22.34	21.95	21.01	24.28	23.44
-21.2	24.47	22.42	23.68	22.70	—	—	11.1	21.80	22.37	22.02	21.07	24.28	23.47
-20.1	24.11	22.55	23.49	22.51	—	—	11.9	21.98	22.56	22.10	21.16	24.28	23.54
-18.9	23.53	22.65	23.32	22.30	24.22	23.60	13.1	22.22	22.70	22.22	21.31	24.40	23.65
-17.8	23.06	22.71	23.12	22.07	24.11	23.48	14.3	22.56	22.72	22.38	21.47	24.39	23.55
-16.6	23.09	22.85	22.94	21.91	24.13	23.44	15.4	22.91	22.58	22.54	21.64	24.40	23.68
-15.4	22.93	22.86	22.76	21.71	24.16	23.56	16.6	23.25	22.70	22.73	21.84	24.42	23.76
-14.3	22.52	22.79	22.55	21.50	24.20	23.56	17.8	23.83	22.84	22.93	22.04	24.50	23.80
-13.1	22.20	22.61	22.41	21.37	24.37	23.50	18.9	23.83	22.80	23.12	22.24	24.68	23.86
-11.9	21.99	22.46	22.25	21.22	24.36	23.62	20.1	24.07	22.69	23.33	22.46	24.78	23.93
-11.1	21.75	22.50	22.10	21.07	24.25	23.41	21.2	24.42	22.60	23.55	22.71	25.01	24.16
-10.5	21.70	22.55	22.01	20.98	24.14	23.27	22.4	24.60	22.58	23.76	22.90	25.17	24.32
-9.9	21.61	22.55	21.92	20.91	23.95	23.20	23.9	24.62	22.48	24.03	23.19	25.33	24.49
-9.3	21.57	22.46	21.86	20.84	23.49	23.14	25.6	24.91	22.43	24.38	23.50	25.47	24.81
-8.7	21.44	22.38	21.80	20.77	23.83	22.97	27.4	25.32	22.45	24.60	23.75	25.71	24.80
-8.1	21.38	22.47	21.71	20.69	23.63	22.79	29.1	25.49	22.21	24.83	24.07	25.82	25.10
-7.6	21.28	22.38	21.61	20.59	23.48	22.67	30.8	—	21.81	25.05	24.19	25.76	—
-7.0	21.17	22.28	21.52	20.49	23.28	22.47	32.6	—	22.08	25.19	24.43	26.14	—
-6.4	20.98	22.17	21.43	20.38	23.04	22.24	34.3	—	22.30	25.44	24.53	—	—
-5.8	20.80	22.02	21.30	20.23	22.76	22.00	36.7	—	22.58	25.48	24.74	—	—
-5.2	20.59	21.88	21.16	20.07	22.45	21.71	39.6	—	23.06	25.74	24.83	—	—
-4.7	20.51	21.72	21.01	19.89	22.10	21.37	42.5	—	23.80	26.10	25.15	—	—
-4.1	20.45	21.53	20.84	19.70	21.69	20.97	45.4	—	23.88	—	—	—	—
-3.5	20.34	21.26	20.57	19.40	21.22	20.49	48.3	—	24.06	—	—	—	—
-2.9	20.17	20.89	20.28	19.10	20.69	19.93	51.2	—	24.38	—	—	—	—
-2.3	19.96	20.52	19.98	18.77	20.16	19.32	54.1	—	24.55	—	—	—	—
-1.7	19.57	20.07	19.61	18.33	19.65	18.67	57.0	—	24.24	—	—	—	—
-1.2	19.21	19.20	19.23	17.85	19.24	18.05	61.4	—	25.04	—	—	—	—
-0.6	18.56	18.56	18.97	17.54	18.95	17.59	67.2	—	25.69	—	—	—	—
0.0	18.20	18.20	18.82	17.39	18.82	17.39		SW	NW	SW	SW	W	W

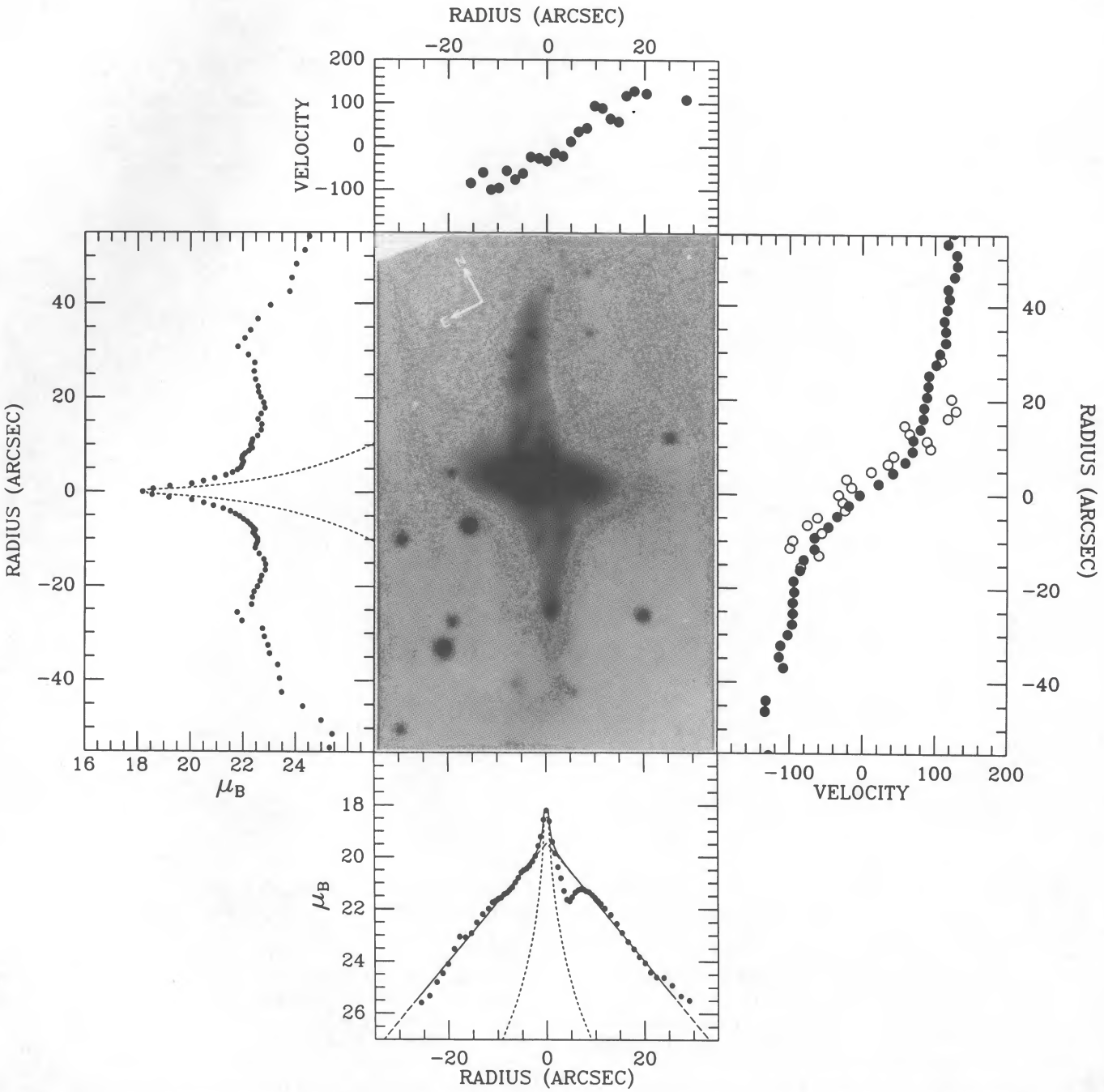

FIG. 2.—Photometric and kinematic data for NGC 4650A. The spatial scale for the panels is approximately the same as the central photograph. The luminosity profiles of the polar ring and the S0 component are shown in the left and bottom panels respectively; their respective rotational velocities are shown in the right and upper panels. The right panel also has the rotational velocities for the S0 component superposed (*open circles*). A comparison of the circular velocities of the two components in the right panel shows that the gravitational potential in NGC 4650A is nearly spherical.

a "resolution width" of 30 km s^{-1} should be subtracted in quadrature to correct the velocity dispersions for template mismatch (Whitmore, Kirshner, and Schechter 1979). The resulting velocities and velocity dispersion profiles are presented in Table 4 and Figure 4 and in Figure 8 below.

III. RESULTS FOR NGC 4650A AND ESO 415-G26

The parameters discussed in this section are summarized in Table 5. The data for A0136-0801 from SWR are included for comparison.

a) NGC 4650A

The peculiar nature of this galaxy was first noted by Sérsic (1967), followed by observations of rotational velocities in the ring by Sérsic and Agüero (1972), Laustsen and West (1980), and Schechter, Ulrich, and Boksenberg (1984, hereafter SUB). NGC 4650A lies in the outskirts of the Centaurus cluster, supporting the finding by Schweizer, Rubin, and Whitmore (1983) that polar-ring galaxies tend to be found near other galaxies. SUB also measured the rotation of the inner 10″ of the "spindle" component but noted that more extended measure-

TABLE 3

EMISSION-LINE VELOCITIES IN THE POLAR RINGS

R	cz (km s^{-1})	V^a (km s^{-1})	R	cz (km s^{-1})	V^a (km s^{-1})
NGC 4650A (P.A. = 158°, $V_0{}^b$ = 2902 km s^{-1}; southeast to northwest)			NGC 4650A—*Continued*		
−60.″0	2790	−122	+27.7	2995	102
−57.8	2781	−132	+30.0	3000	107
−55.4	2784	−129	+32.3	3007	115
−46.2	2779	−134	+34.7	3007	115
−43.9	2780	−133	+37.0	3005	113
−37.0	2802	−109	+39.3	3009	117
−34.7	2797	−115	+41.6	3012	120
−32.3	2799	−113	+43.9	3010	118
−30.0	2808	−103	+46.2	3018	127
−27.7	2813	−97	+48.5	3022	131
−25.4	2814	−96	+50.8	3021	130
−23.1	2814	−96	+53.1	3010	118
−20.8	2816	−94	+55.4	3017	126
−18.5	2815	−95	+57.8	3001	108
−16.2	2823	−86			
−13.9	2828	−81			
−11.6	2842	−66	ESO 415-G26 (P.A. = 92°, V_0 = 4579 km s^{-1}; east to west)		
−9.2	2842	−66			
−6.9	2859	−47			
−4.6	2870	−35	−32.″9	4762	194
−2.3	2885	−19	−30.5	4760	192
0.0	2906	−4	−28.2	4767	200
+2.3	2922	22	−25.8	4765	198
+4.6	2940	42	−23.4	4763	195
+6.9	2956	59	−21.1	4754	186
+9.2	2965	69	−18.7	4753	185
+11.6	2966	70	−17.4	4756	188
+13.9	2975	80	−15.0	4755	187
+16.2	2979	84	−11.4	4753	185
+18.5	2980	85	+16.9	4402	−188
+20.8	2983	89	+19.4	4401	−189
+23.1	2985	91	+20.1	4413	−176
+25.4	2986	92	+21.7	4399	−191

[a] Rotational velocity corrected for inclination and relativity using eq. (1). The values for NGC 4650A also include a correction for the warp. See Table 5 for a summary of the corrections.

[b] Systemic heliocentric velocity determined by averaging the data in the outer regions.

ments would be needed to establish whether it was definitely an S0 disk. Our own observations agree very well with SUB but extend more than twice as far out. Our emission-line velocities in the ring are also in good agreement with previous observations (with offsets required for Sérsic and Agüero 1972 and Laustsen and West 1980) but extend ~50% farther and have much less scatter. Figure 2 presents the photometric and kinematic data for NGC 4650A. The spatial scale of each panel is approximately the same as that of the photograph, and the various profiles have been oriented roughly parallel to the galaxy components to which they refer.

i) *Photometry*

Figure 2 shows a CCD image of NGC 4650A in the *B* passband. Figure 3 shows the same image displayed at different contrast levels (Fig. 3*e* uses a logarithmic contrast scale). This galaxy is almost a carbon copy of A0136-0801 but is better resolved because of its smaller distance. Two bright knots are seen at nearly equal distances from the nucleus in the polar ring. These are probably caused by the warping of a narrow ring, as advocated by Laustsen and West (1980). In this interpretation the knots are produced where the two sides of the narrow ring are aligned with our line of sight. If this is correct, the peak brightness of the knots should be about twice as bright as in regions where the ring is not superposed; this appears to be the case. A comparison of the surface brightness in the two knots with 10 positions in the ring yields a ratio of 1.91 ± 0.06. The ratio is probably below 2.0 because some of the light in the distant part of the ring is absorbed by dust in the front part. Other polar-ring galaxies show similar bright knots, notably AM 2020-5050, II Zw 73, ESO 603-G21, and ESO 474-G26. However, in most cases the enhancement is near the end of the ring where the ring runs nearly parallel to our line of sight. Several of these systems show a lobe only on one side, possibly due to the presence of dust or the uneven distribution of material along the ring.

At the faintest intensity levels one sees extensive evidence for disordered nebulosity in the outer regions, especially in the northwest corner and in the southeast along a line running parallel to the polar ring but offset slightly above it. This material may consist of stellar debris accreted from the outskirts of the nearby galaxy NGC 4650 (see § IV*b* and Fig. 9 below). The surface brightness of the brightest debris in the northwest corner is ~25.4*B* mag arcsec^{-2}. Part of it is just barely visible on the image shown by Laustsen and West (1980).

The luminosity profile along the major axis of the S0 component is shown in the bottom panel of Figure 2. The central

TABLE 4

STELLAR VELOCITIES IN THE S0 DISKS

R	cz (km s^{-1})	σ (km s^{-1})	V[a] (km s^{-1})
NGC 4650A (P.A. = 63°, V_0[b] = 2909 km s^{-1}; northeast to southwest)			
−15″.5	2837 ± 21	...	−85
−13.0	2858 ± 18	...	−60
−11.4	2824 ± 13	57 ± 20	−100
−9.8	2827 ± 13	60 ± 19	−96
−8.2	2861 ± 12	41 ± 20	−56
−6.5	2844 ± 11	50 ± 18	−76
−4.9	2856 ± 13	70 ± 18	−62
−3.3	2889 ± 11	55 ± 16	−24
−1.6	2886 ± 12	74 ± 16	−27
0.0	2881 ± 10	70 ± 13	−33
+1.6	2896 ± 9	86 ± 13	−15
+3.3	2890 ± 11	97 ± 14	−22
+4.9	2919 ± 12	76 ± 15	+12
+6.5	2939 ± 16	...	+35
+8.2	2946 ± 18	...	+43
+9.8	2989 ± 15	87 ± 24	+94
+11.4	2985 ± 11	69 ± 23	+89
+13.0	2964 ± 16	...	+65
+14.7	2958 ± 16	...	+58
+16.3	3009 ± 22	...	+118
+17.9	3019 ± 24	...	+129
+20.4	3014 ± 27	...	+123
+28.5	3002 ± 22	...	+109
ESO 415-G26 (P.A. = 16°, V_0 = 4527 km s^{-1}; northeast to southwest)			
−22″.8	4383 ± 17	...	−170
−19.6	4394 ± 20	...	−157
−17.9	4369 ± 17	...	−186
−16.3	4380 ± 13	...	−173
−14.7	4406 ± 13	78 ± 24	−143
−13.0	4400 ± 10	49 ± 22	−150
−11.4	4373 ± 11	69 ± 23	−181
−9.8	4397 ± 14	88 ± 24	−153
−8.2	4419 ± 9	115 ± 15	−127
−6.5	4430 ± 12	134 ± 18	−114
−4.9	4434 ± 8	65 ± 16	−110
−3.3	4449 ± 6	97 ± 10	−92
−1.6	4496 ± 7	137 ± 10	−37
0.0	4549 ± 8	130 ± 11	+26
+1.6	4605 ± 6	113 ± 9	+92
+3.3	4623 ± 6	98 ± 10	+113
+4.9	4652 ± 7	112 ± 12	+147
+6.5	4647 ± 9	107 ± 16	+141
+8.2	4671 ± 8	69 ± 16	+170
+9.8	4687 ± 13	88 ± 24	+188
+11.4	4697 ± 12	100 ± 21	+200
+13.9	4669 ± 12	98 ± 22	+167
+17.1	4640 ± 15	...	+133
+22.0	4654 ± 20	...	+150
ESO 415-G26 (P.A. = 92°, V_0 = 4557 km s^{-1}; southeast to northwest)			
−4″.9	4567 ± 42	...	+10
−3.3	4534 ± 13	116 ± 21	−23
−1.6	4565 ± 8	128 ± 12	+8
0.0	4560 ± 7	130 ± 10	+3
1.6	4564 ± 7	124 ± 11	+7
3.3	4560 ± 11	103 ± 19	+3
4.9	4582 ± 27	...	+25

[a] Rotational velocity corrected for inclination, relativity, and line-of-sight projection. See Table 5 for a summary of the corrections.

[b] Systemic heliocentric velocity determined by averaging the data in the outer regions.

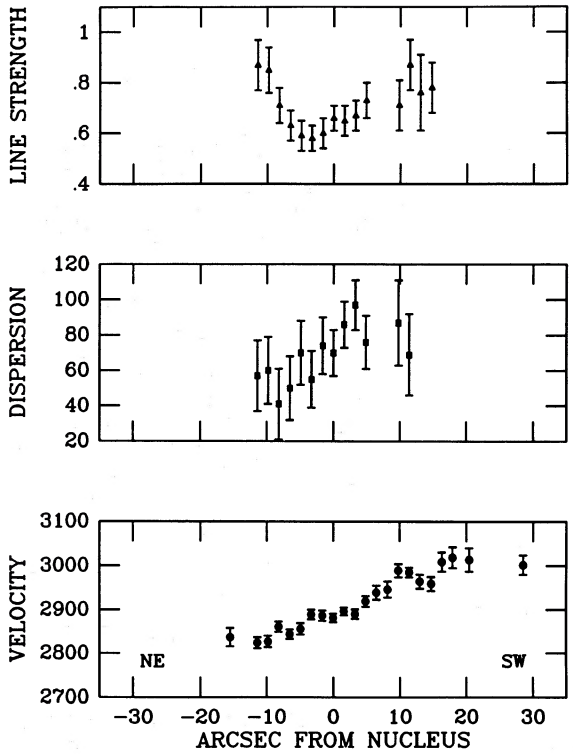

FIG. 4.—Line strength index, rotational velocity, and velocity dispersion along the major axis of the S0 componentof NGC 4650A.

region shows a well-defined bulge component, while the intermediate region has an exponential profile. The southwest side shows the absorption from the polar ring at a radius of ∼5″.

A bulge decomposition following the method outlined by Whitmore and Kirshner (1981) indicates a moderately faint bulge, with $M_B = -17.3 \pm 0.5$. The bulge-to-disk ratio is only 0.14, typical of an Sc galaxy. Separate decompositions were made using the major axis, minor axis, and effective radius [$(ab)^{1/2}$] profiles. The three methods yielded the same bulge luminosity to within ∼0.3 mag. For regions on the southwest side which were affected by the dust lane, brightness values from the northeast side were substituted. The absolute magnitude of the ring is -18.2 ± 0.5. Therefore, the relative fractions of light in the bulge, disk, and ring are 10%, 68%, and 22% respectively.

The ellipticity of the S0 component is 0.58 at $B = 21.5$ mag arcsec^{-2}. This alone suggests that it is a disk system, since E6 galaxies are rare.

While we do not have an image of NGC 4650A in V, Sérsic and Agüero (1972) measured a fairly blue color for the system, especially the ring. They find a total $B-V = 0.60$ (corrected by us for reddening according to Burstein and Heiles 1985), a $B-V = 0.81$ for the inner component, and a $B-V = -0.09$ for the outer filaments of the ring. The very blue color of the ring corroborates the presence of recent star formation, inferred more directly from the presence of emission lines characteristic of H II regions. Laustsen and West (1980) also find that the ring is "considerably bluer" than the S0 component.

ii) *Spectroscopy*

The emission-line rotation curve of the polar ring (shown in the right panel of Fig. 2) is similar to the rotation curve of any normal spiral galaxy, although it is measured vertically to the

TABLE 5

DATA FOR THE PROGRAM GALAXIES

Parameter	NGC 4650A	ESO 415-G26	A0136-0801
General properties:			
Heliocentric velocity (km s^{-1})	2904 ± 4	4560 ± 13	5528 ± 4
Velocity relative to Local Group[a] (km s^{-1})	2667	4474	5576
Distance (H_0 = 50) (Mpc)	53.3	89.5	111.5
Apparent B mag	14.27 ± 0.4	14.60 ± 0.2	16.6 ± 0.8
Absolute B mag[b]	−19.86 ± 0.4	−20.16 ± 0.2	−18.6 ± 0.8
Total $B-V$	0.60[c]	0.91	...
Scale (kpc arcsec^{-1})	0.259	0.434	0.541
Mass-to-light ratio in B for inner region	0.7 ± 0.2 within 14″	6.3 ± 1.3 within 18″	14 ± 8 within 15″.3
Mass-to-light ratio in B within last observed point	4.5 ± 0.9 within 60″	9.3 ± 1.8 within 32″.9	25 ± 14 within 31″.3
Effective radius	19″	18″	6″.5
Same (kpc)	4.9	7.8	3.5
Comparison radius	14″	18″	8″
Same (kpc)	3.6	7.8	4.3
V_{ring}/V_{disk}	0.89 ± 0.18	1.04 ± 0.14	0.98 ± 0.17
Flattening of gravitational potential c/a	0.86 ± 0.21	1.05 ± 0.17	0.98 ± 0.20
S0 Component:			
Radii at B = 25 mag arcsec^{-2} ($r_{25} \times R_{25}$)	10″.3[d] × 24″.5	19″.5 × 30″.4	6″.8 × 12″.2
Same (kpc)	2.7 × 6.3	8.5 × 13.2	3.7 × 6.6
Major axis position angle:			
Inner	61° ± 1°	17° ± 1°	138° ± 1°
Outer	60° ± 1°	17° ± 1°	...
Debris	...	53° ± 5°	...
Absolute B magnitude:			
Bulge	−17.3 ± 0.5	−19.0 ± 0.4	−16.9 ± 0.4
Disk	−19.4 ± 0.2	−19.7 ± 0.4	−17.6 ± 0.6
$B-V$	0.81[c]	1.02 ± 0.03 within 2″.9	...
	...	0.90 ± 0.08 in halo	...
Bulge-to-disk ratio	0.14	0.52	$\gtrsim$0.5
Effective radius of bulge	1″.1	2″.5	0″.7
Same (kpc)	0.3	1.1	0.4
Scale length for disk	4″.79	7″.61	2″.30
Same (kpc)	1.24	3.30	1.24
$(\partial \ln \rho)/(\partial \ln R)$	2.92	2.37	3.48
Central velocity dispersion σ_0[e] (km s^{-1})	77 ± 5	127 ± 3	67 ± 7
V/σ_0	0.96 ± 0.12	1.14 ± 0.08	2.07 ± 0.34
Ellipticity	0.58 at B = 21.5	0.66 at B = 22.5	0.45 at B = 25
Inclination i	68° ± 4°	74° ± 4°	58° ± 5°
Velocity corrections:			
1/sin i	1.079 ± 0.03	1.040 ± 0.02	1.179 ± 0.06
1/(1 + z)	0.991	0.985	0.982
Line of sight	1.10 ± 0.11	1.15 ± 0.11	1.05 ± 0.11
Asymmetrical drift	1.067 ± 0.05	1.067 ± 0.07	1.011 ± 0.01
Total correction	1.255 ± 0.12	1.257 ± 0.13	1.229 ± 0.13
Corrected rotational velocity at comparison radius V_{disk} (km s^{-1})	88 ± 9 at 14″	178 ± 11 at 18″	148 ± 19 at 8″
Polar ring component:			
Radius	54″.8	19″.5	...
Same (kpc)	14.2	8.5	...
Inner	...	...	10″
Same (kpc)	...	...	5.4
Outer	...	...	32
Same (kpc)	...	...	17.3
Major axis position angle:			
Inner	161° ± 1°	93° ± 1°	52° ± 1°
Outer	157° ± 1°	...	...
Inclination	85°[f] ± 5°	68° ± 2°	79° ± 2°
Absolute B magnitude	−18.2 ± 0.5	−15.5 ± 1.0	−17.6 ± 0.6
$B-V$	−0.09[c]	0.65 ± 0.08	...
Velocity corrections:			
1/sin i	1.004	1.079 ± 0.02	1.019
1/(1 + z)	0.991	0.985	0.982
Warped disks	1.10 ± 0.10[g]	1.0 ± 0.0	1.0 ± 0.0
Total correction	1.094	1.063	1.001
Corrected rotational velocity at comparison radius V_{ring} (km s^{-1})	78 ± 3 at 14″	186 ± 2 at 18″	145 ± 9 at 8″
Maximum rotational velocity V_{max} (km s^{-1})	122 ± 6 at 60″	193 ± 4 at 32″.9	168 ± 10 at 31″.3

[a] Calculated using $V_{LG} = V + 300 \sin l \cos b$.
[b] A_B = 0.00 used for ESO 415-626 and A0136-0801, A_B = 0.49 used for NGC 4650A (Burstein and Heiles 1985).
[c] From Sérsic and Agüero 1972, using absorption and reddening corrections from Burstein and Heiles 1982.
[d] Minor axis based on major axis and ellipticity.
[e] Average of inner three measurements (4″.8) in both major and minor axis when possible.
[f] From Laustsen and West 1980.
[g] Typical correction factor for various models of a warped ring.

S0 disk and extends to 2.4 times the radius at the 25th B isophote (R_{25}) of that disk (note from Table 3 that velocities were measured out to 60".0 on the southeast side and 57".8 on the northwest side of the ring, farther than plotted in Fig. 2). This is much farther than can normally be measured using optical emission lines in a spiral galaxy. The rotational velocities show no sign of falling in a Keplerian manner but are actually slightly rising even at the most distant point. This shows the dominant role of dark matter in the outer halo. Since the polar ring is warped, it was impossible to align the slit at all radii. We therefore computed corrections using the method described in Burbidge and Burbidge (1975). Since the warp makes these corrections uncertain at any particular radius, we have adopted a typical correction of 1.10 ± 0.10 at all radii. The maximum rotational velocity is then $V_{max} = 122 \pm 6$ km s^{-1} at 60" (15.5 kpc), which would be typical of an Sc galaxy with the same absolute magnitude as NGC 4650A. The mass within the outermost radius is $M(15.5 \text{ kpc}) = 5.4 \times 10^{10} M_\odot$, with a corresponding value of the mass-to-light ratio of $M/L(15.5 \text{ kpc}) = 4.5 \pm 0.9$. Within the inner 14" of the S0 disk (the comparison radius discussed in § IV*a*), $M/L(3.6 \text{ kpc}) = 0.7 \pm 0.2$. While this is quite low, even for an Sc galaxy, it is consistent with the various indications of recent star formation.

The rotation curve of the S0 component is shown in Figure 4. It extends to $\sim 0.9 R_{25}$ (22" or 5.7 kpc). The curve flattens in the outer regions, clearly showing that the system cannot be a tumbling bar with a solid-body rotation curve. The central velocity dispersion is $\sigma_0 = 77 \pm 5$ km s^{-1}, while the mean velocity dispersion for all the data is 70 ± 4 km s^{-1}. These values agree with Whitmore and Kirshner's (1981) central value of 80 km s^{-1} for a bulge with the same magnitude as that of NGC 4650A.

The value of V/σ_0 for the S0 component of NGC 4650A is 0.96 ± 0.12. This high value also rules out the possibility that the inner component is a tumbling bar (Richstone and Potter 1982).

Figure 5 shows part of the spectra of the template star HD 19555 (K1 III), and of ESO 415-G26 and NGC 4650A. While ESO 415-G26 shows a normal spectrum for an S0 galaxy, NGC 4650A shows a much earlier type spectrum, including strong Balmer absorption at Hγ. This suggests a recent burst of star formation in this galaxy, as already pointed out by Schechter, Ulrich, and Boksenberg (1984).

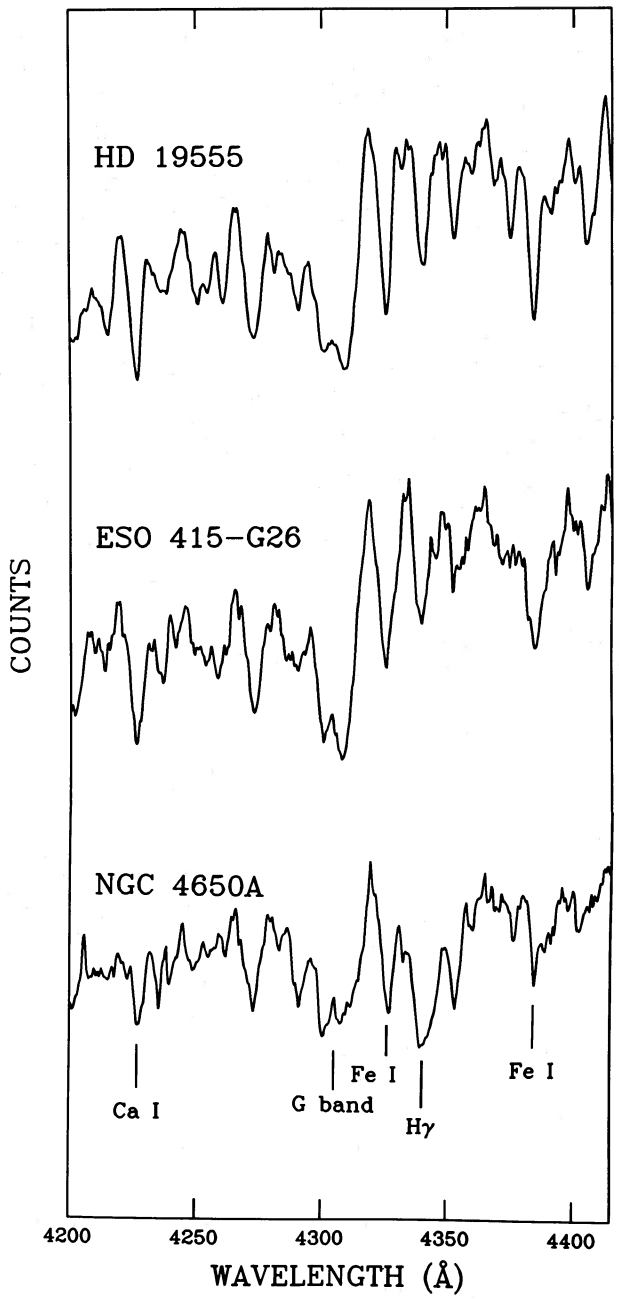

FIG. 5.—Spectra of the template star HD 19555 (K1 III) and the polar-ring galaxies ESO 415-G26 and NGC 4650A. Note the strong Hγ absorption line in NGC 4650A.

b) ESO 415-G26

Unlike A0136-0801 and NGC 4650A, the outer ring of ESO 415-G26 (= MCG-05-07-001 = AM 0226-3206) is very faint. It was discovered by Arp and Madore (1986) and observed in more detail by Schechter and Kristian (1984) and van Gorkom, Schechter, and Kristian (1987). They found that a CCD image of this system revealed "a faint, asymmetric envelope extending well beyond the main body of the galaxy." They suggest that the material is the stellar debris left from the merger of an S0 galaxy and a smaller gas-rich galaxy. Figure 6 presents our photometric and kinematic data in the same format as Figure 2.

i) *Photometry*

Figure 6 shows an image of ESO 415-G26 in the B passband. Figure 7 (Plate 13) shows four reproductions of the same B image at different contrast levels to show various features (Fig. 7*a* uses a logarithmic contrast scale). The bright part of the ring appears very narrow ($\sim 2".0 \pm 1".0$ after deconvolution for seeing) and is faint near the end points, unlike most other polar rings. This faintness may be caused by a warped disk covering the outer region, or the density of the material along the ring may actually vary.

The faint, asymmetric halo reported by van Gorkom, Schechter, and Kristian (1987) is clearly shown in Figures 7*c* and 7*d*. A prominent loop is seen on the north side $\sim 43"$ from the nucleus, and ripples ("shells") are seen in the northeast at $\sim 63"$ and $\sim 88"$, and possibly in the west at $\sim 52"$. The major axis of the faintest material is $53° \pm 10°$, which differs by 36° from the major axis of the S0 component. This outer debris appears in the luminosity profile of the S0 component as a

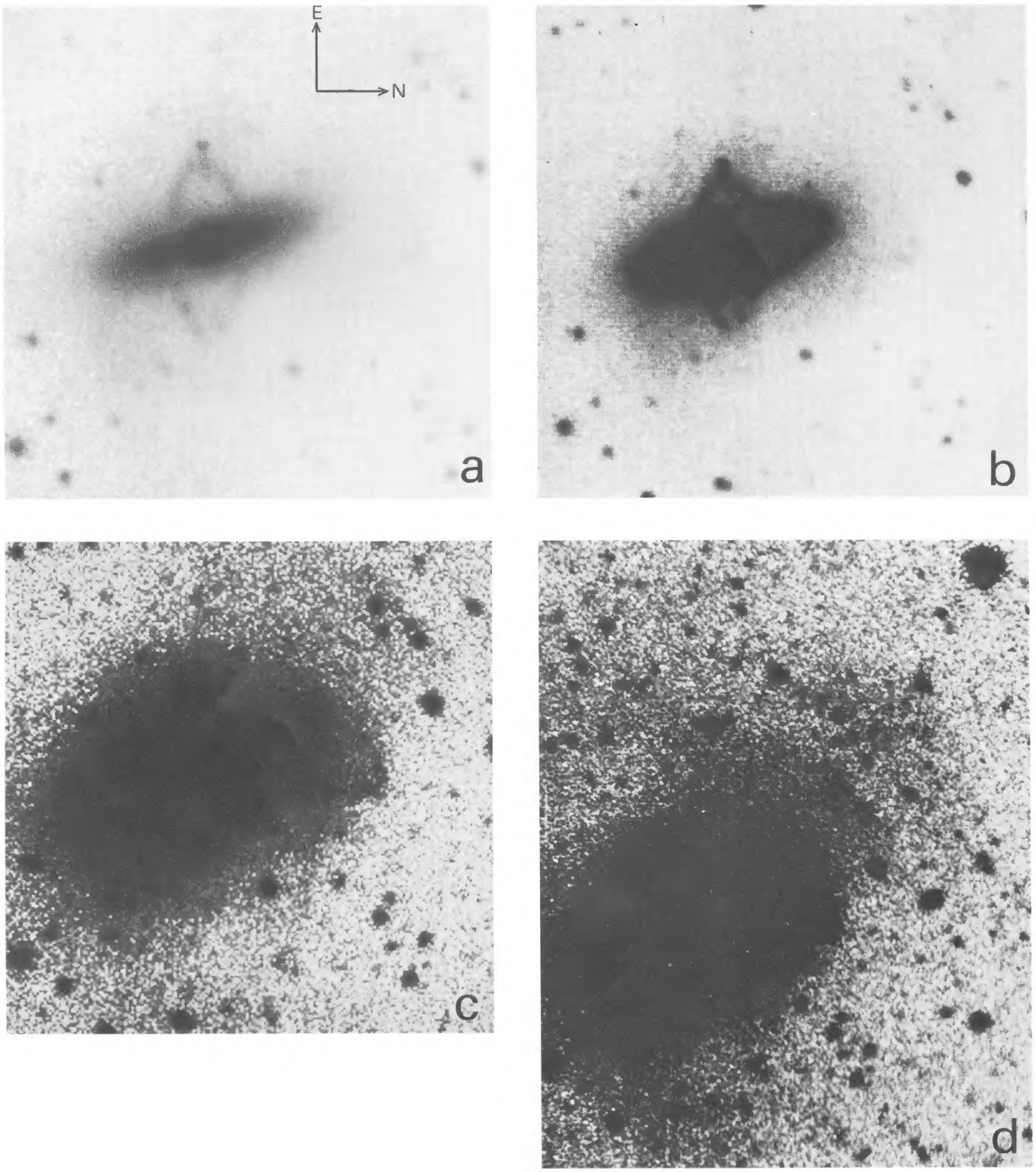

FIG. 7.—Blue image of ESO 415-G26 displayed at four different contrasts; (*a*) uses a logarithmic gray scale

WHITMORE, MCELROY, AND SCHWEIZER (*see* page 447)

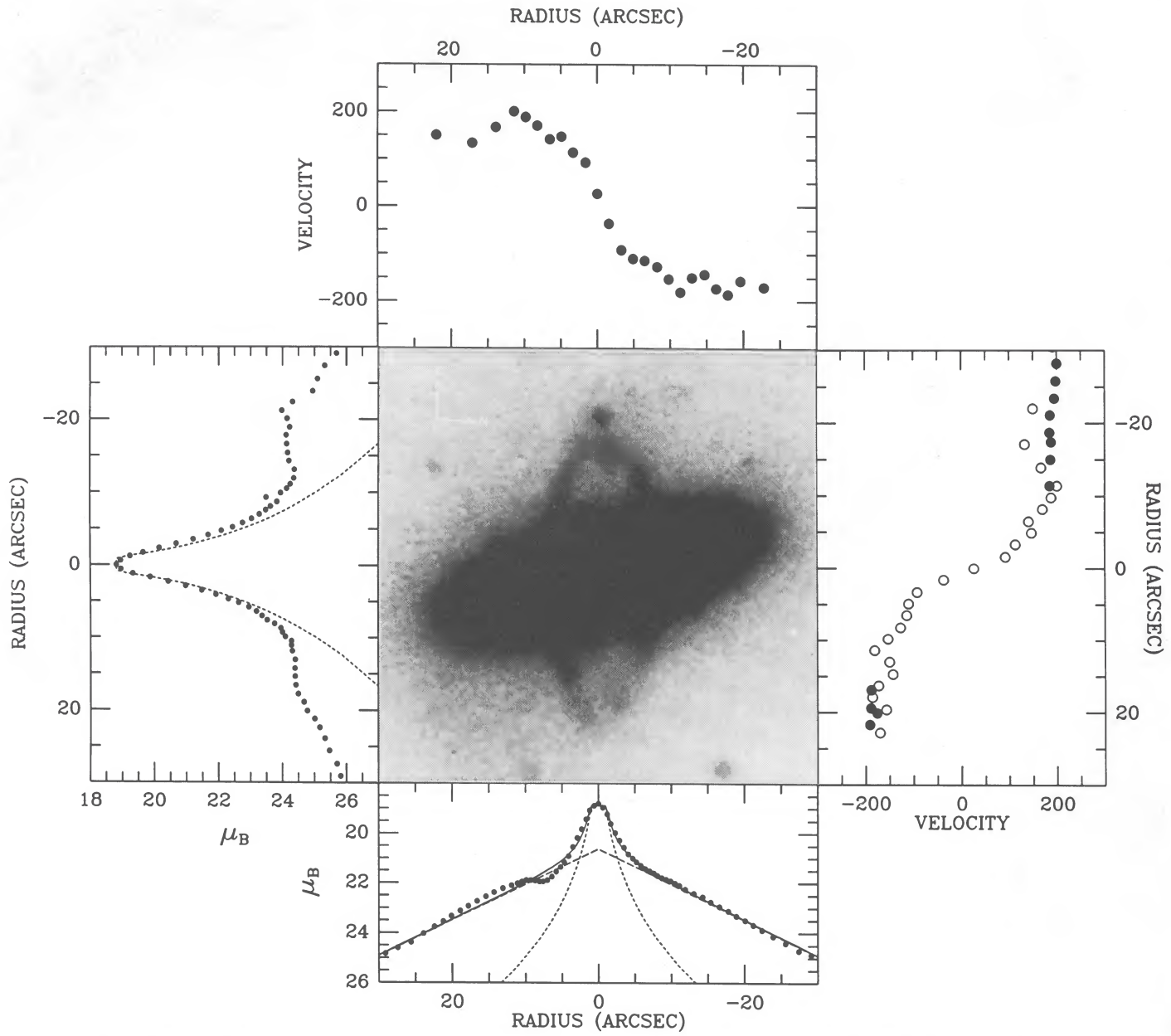

FIG. 6.—Photometric and kinematic data for ESO 415-G26. Same display scheme as Fig. 2. A comparison of the circular velocities of the two components in the right panel shows that the gravitational potential in ESO 415-G26 is nearly spherical.

sharp upturn at ~40″ on either side (see Table 3; Fig. 6 does not extend this far). This makes ESO 415-G26 one of only a few galaxies with shells which do not have an elliptical galaxy as the central component (Hernquist and Quinn 1986). The material is quite red ($B-V = 0.90 \pm 0.08$), characteristic of an old stellar population rather than a young population. This supports the idea outlined in SWR that during the merging process, the stellar component of the accreted companion would disperse into the halo while the gas clouds would experience collisions and quickly settle into a new disk or ring.

The luminosity profile along the major axis of the S0 disk of ESO 415-G26 is shown in the bottom panel of Figure 6. The central bulge is quite prominent; a decomposition of both the major axis profile and the minor axis profile yields a bulge absolute magnitude of $M_B = -19.0 \pm 0.4$ and a bulge-to-disk ratio of $B/D = 0.5$ (typical of an Sa or Sb galaxy). The disk follows an exponential profile quite well in the region from 10″ to 40″, where the outer debris starts showing up. The relative fractions of light in the bulge, disk, and ring are 34%, 65%, and 1% respectively.

The apparent ellipticity of the S0 component is 0.66 at $B = 22.5$ mag arcsec^{-2}. This again suggests that it is a disk system, since E7 galaxies are extremely rare. An even thinner disk can be seen in Figure 7*a*.

The ring is considerably bluer ($B-V = 0.65 \pm 0.08$) than the S0 disk ($B-V = 1.02 \pm 0.03$ within the central 2.″9) but is not nearly as blue as reported for NGC 4650A by Sérsic and Agüero (1972; $B-V = -0.09$).

ii) *Spectroscopy*

The rotation curve of the polar ring of ESO 415-G26 (shown in the right panel of Fig. 6) extends nearly as far (in linear measure) as that of NGC 4650A. The east side of the rotation curve is flat and extends well beyond the observed limits of the

ring. The maximum rotational velocity is 193 km s^{-1} within 32.″9 (14.3 kpc). The mass within the outermost radius is $M(14.3\ \text{kpc}) = 1.2 \times 10^{10}\ M_\odot$, with a corresponding value of the mass-to-light ratio in B of $M/L(14.3\ \text{kpc}) = 9.3 \pm 1.8$. Within the inner 18″ of the S0 disk (the comparison radius), the mass is $M(7.8\ \text{kpc}) = 6.3 \times 10^{10}\ M_\odot$, and $M/L(7.8\ \text{kpc}) = 6.3 \pm 1.3$.

The rotation curve of the S0 component of ESO 415-G26 is shown in Figure 8. It extends to $\sim 0.8 R_{25}$. A definite turnover is seen in the outer regions, suggesting again that the system cannot be a tumbling bar. The central velocity dispersion is $\sigma_0 = 127 \pm 3$ km s^{-1}, considerably higher than for NGC 4650A or A0136-0801. This is consistent with the brighter bulge ($M_B = -19.0$); the relation for bulges of spiral galaxies would predict $\sigma_0 = 123$ km s^{-1} (Whitmore and Kirshner 1981). The mean velocity dispersion for all the data is $\sigma = 102 \pm 5$ km s^{-1}. The value of V/σ_0 for ESO 415-G26 is 1.14 ± 0.08 km s^{-1}.

IV. DISCUSSION

In the following discussion, we concentrate on two questions that our data can help answer: How is the mass, including the dark matter, distributed in polar-ring galaxies? And how old are the polar rings? We also briefly speculate about the formation histories of the three polar-ring galaxies studied here.

a) Distribution of Dark Matter in Polar-Ring Galaxies

There are several indirect arguments for the sphericity of the dark halo in disk systems. Tubbs and Sanders (1979) argue that the observed warps in the outer regions of disk galaxies can persist only if the potential there is nearly spherically symmetric. Whitmore and Kirshner (1981) note that a comparison between the central velocity dispersion and the rotation in the outer disk of bulge-dominated systems yields a value of $V/\sigma_0 = 1.6$, close to the value of 1.4 expected in a nearly spherical potential. Monet, Richstone, and Schechter (1981) find that the shape of the halo of the Milky Way may also be rather spherical. While all these arguments are suggestive of a nearly spherical potential, the direct measurement made possible by polar-ring galaxies provides a much stronger case.

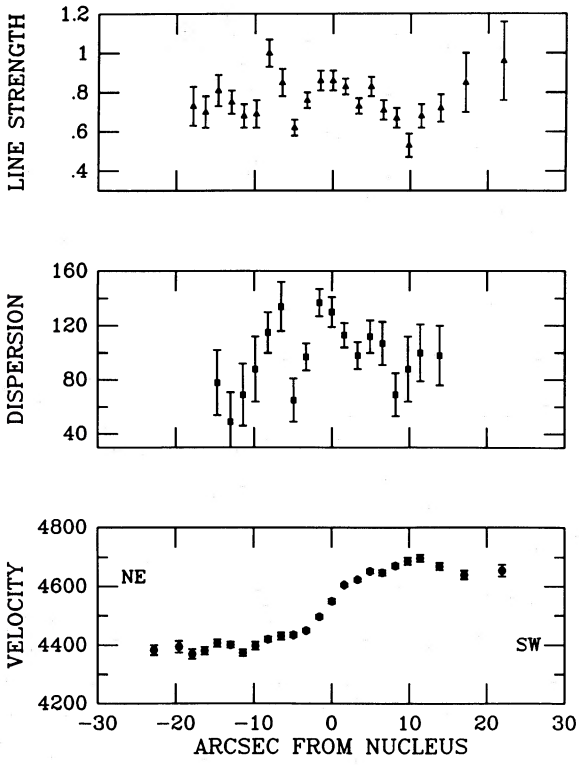

FIG. 8.—Line strength index, rotational velocity, and velocity dispersion along the major axis of the S0 component of ESO 415-G26.

The shape of the gravitational potential can be determined from a straightforward comparison of the rotational velocities in the polar rings and S0 disks. If all the mass were concentrated in the S0 disk, a particle above the disk would feel a smaller gravitational force than a particle at the same radius within the disk. SWR show that for a Kuzmin (1956) disk the polar velocities are lower than the equatorial velocities within the disk by 20%–40% over a wide range of distances from the center. For the scale-free potential given by Monet, Richstone, and Schechter (1981) and a mass distribution concentrated in a flat disk, the velocity ratio is $V_{\text{pol}}/V_{\text{equ}} = 0.58$. A tabulation of polar velocities for two potential functions and various flattenings is given by Katz and Richstone (1984; but see footnote 3 below).

i) *Velocity Corrections*

Before we can estimate the shape of the gravitational potential by comparing the rotational velocities in the rings with those in the S0 disks, some of the corrections applied to the velocities measured from absorption lines in the S0 disk need further discussion. The accuracy of the absorption-line velocities themselves is not at issue. Thanks to the Fourier quotient technique, absorption-line measurements are now quite routine, and the internal errors for our setup are generally less than 10 km s^{-1}.

However, four corrections must be applied to the measured velocities to convert them to circular velocities in the plane of the disk. Two of these corrections are straightforward and unproblematic: the $1/(1+z)$ correction for relativistic effects and the $1/\sin i$ correction for the inclination of the S0 disk against the plane of the sky (eq [1]). Inclinations were estimated via the procedure of Heidmann, Heidmann, and de Vaucouleurs (1971) and assuming an intrinsic disk thickness of $q_0 = 0.2$. The resulting values of the first two corrections and the estimated errors of the inclination correction are given in Table 5.

The remaining two corrections, however, are more difficult to evaluate. One is the correction for line-of-sight integration through the presumably transparent S0 disk, and the other is a correction for pressure support in the S0 disk. We now discuss these two corrections in turn.

Velocities measured along the apparent major axis of an S0 disk seen nearly edge-on represent luminosity-weighted averages for all stars along the line of sight; yet most of these stars orbit at some angle with respect to the line of sight. A determination of the true rotation of the disk therefore requires a correction for integration along the line of sight, which is a function of the luminosity profile, the shape of the intrinsic rotation curve, the dependence of rotation on the height above the plane, and the inclination of the disk. The problem is compounded by the fact that the S0 component itself is composed of two subcomponents, a bulge and a disk, each with its own luminosity profile and intrinsic rotation curve.

For simplicity, assume that effects from the bulge of the S0 galaxy can be ignored. The luminosity profiles in Figures 2 and

6 show that this assumption is reasonable if we use the outer region of the S0 disk to make the velocity comparison. This comparison radius is at ~ 23 mag arcsec^{-2} in B for all three of our polar-ring galaxies. We can then bracket the necessary correction as follows. If the S0 disk were infinitely thin and not observed exactly edge-on, no correction would be necessary, since our line of sight would cross the disk at a single point. This is the assumption usually made for emission-line rotation curves. If, on the other hand, the S0 disk is thick and seen exactly edge-on, then an upper limit can be set by using a formula developed by Young *et al.* (1978) for an edge-on elliptical galaxy. Assuming a flat rotation curve and a power-law luminosity profile with $d \ln L/d \ln R \approx -3.0$, which is typical for our S0 galaxies in the region where the comparison is made, we calculate a maximum correction factor of 1.3. The true correction is smaller if the rotation curve is still rising and the S0 disk is not seen exactly edge-on.

In SWR, we calculated a correction for an exponential disk seen exactly edge-on by solving an integral equation for the intrinsic rotation curve numerically; this gave a correction factor of 1.15 at the comparison radius used for A0136-0801. Since the comparison radius for all three of our polar-ring galaxies is almost the same ($0.61 \pm 0.04 R_{25}$), this correction factor is reasonable for the other two systems. The main difficulty is the assumption that the S0 disk is seen exactly edge-on. This is probably a good approximation for NGC 4650A, and especially for ESO 415-G26, since their S0 components appear quite thin. In A0136-0801 the disk inclination is more face-on and the line-of-sight correction is correspondingly smaller (note, however, that the factor $1/\sin i$ needed to correct for inclination tends to compensate for the smaller line-of-sight correction). We have therefore assumed correction factors of 1.10, 1.15, and 1.05 for NGC 4650A, ESO 415-G26, and A0136-0801 respectively. Our estimated uncertainty is 10%, based primarily on our upper and lower bounds for the correction factor.

The last and most difficult correction to evaluate has to do with the random motions of stars in the S0 disk. The rotation velocity of stars $V_{\rm disk}$, obtained after applying the previous three corrections, is not the same as the circular velocity $V_{\rm cir}$ that a perfectly cold disk of particles (e.g., a gas disk) would have. Yet it is the latter velocity which we should use to compare with the rotational velocity in the polar ring. The two velocities are related through the stellar-dynamical equation

$$V_{\rm cir}^2 = V_{\rm disk}^2 - \sigma_r^2 \frac{\partial \ln \rho}{\partial \ln R} \qquad (3)$$

that explains the asymmetrical drift of stars in the solar neighborhood (e.g., Oort 1965, especially § 4.5). While values of $(\partial \ln \rho)/(\partial \ln R)$ can be estimated from our photometry (see Table 5), the values of σ_r at the comparison radii are unknown. Our experience with numerical experiments using the Fourier quotient technique indicates that the method fails for velocity dispersions below $\sim 25\%$ of the FWHM of a comparison line. Since our FWHM was ~ 250 km s^{-1}, this corresponds to ~ 60 km s^{-1} in our case. The velocity dispersions in the disks are almost certainly lower, so we must find another way of estimating the true velocity dispersion.

A reasonable method of making this estimate is provided by the equation

$$\sigma_z(R) = \sigma_z(0) \exp(-R/2h), \qquad (4)$$

adopted from van der Kruit and Freeman (1986), where $\sigma_z(R)$ is the z-component of the stellar velocity dispersion at a radius R, $\sigma_z(0)$ is the central velocity dispersion of the disk, and h is the exponential scale length of the disk (given in Table 5). Following Illingworth and Schechter (1982), we assume $\sigma_z = \sigma_r$, so that equations (3) and (4) can be combined to estimate the asymmetrical drift correction $V_{\rm cir}/V_{\rm disk}$. Our central velocity dispersions are more appropriate for the bulge than the disk, so this equation should provide a slight overestimate, since the bulge dispersion is larger than the disk dispersion for most reasonable models.

We can test equation (4) using three galaxies where both $\sigma(R)$ and $\sigma(0)$ have been measured. In NGC 3115, the central dispersion is 247 km s^{-1} (Whitmore, McElroy, and Tonry 1985) and $h = 47''.9$ (Tsikoudi 1979). Equation (4) then predicts $\sigma_z(100'') = 87$ km s^{-1}, compared to an observed value of 50 km s^{-1} (Illingworth and Schechter 1982). In NGC 5247, van der Kruit and Freeman (1986) find a central dispersion of 75 km s^{-1} (averaging their inner three measurements) and $h = 40''$ (3.1 kpc). This results in $\sigma_z(87'') = 25$ km s^{-1}, compared to a measurement of 28 km s^{-1}. The lack of a sizable bulge component in this galaxy probably explains the better agreement than in NGC 3115. Finally, in our own Galaxy, if we assume that $\sigma_z(0) = 120$ km s^{-1} based on Frenk and White's (1980) analysis of globular clusters, and $h = 3.55$ kpc (de Vaucouleurs and Pence 1978), then $\sigma_z(8.0$ kpc$) = 39$ km s^{-1}. This is slightly greater than the Jahreiss and Wielen (1983) estimate of 25 km s^{-1} for the local neighborhood.

These three cases give us some confidence that equation (4) can be used to provide values of σ_r for equation (3). The predicted values of σ_r at the comparison radii are then 18 km s^{-1} (NGC 4650A), 39 km s^{-1} (ESO 415-G26), and 12 km s^{-1} (A0136-0801). The corresponding corrections for asymmetrical drift are 1.067, 1.067, and 1.011 respectively. These may be slight overestimates, as discussed above, but in any case it is reassuring to find the correction is quite small.

ii) *Extent of Dark Halo*

In all three galaxies, the rotation curves of the polar rings are flat or keep rising with increasing radius out to the last observed point. The limiting radii are $R_{\rm max} = 60'' = 2.4 R_{25}$ for NGC 4650A, $32''.9 = 1.1 R_{25}$ for ESO 415-G26, and $31''.3 = 2.6\ R_{25}$ for A0136-0801 (see Table 5; note that in both Figs. 2 and 6 the outermost few points are not plotted because they fall outside the display frames). Therefore, the rings appear to rotate in a manner similar to the disks of spiral galaxies, although here the rings extend nearly perpendicular to the S0 disks. The distances reached by our measurements are much greater relative to R_{25} than the distances out to which one can normally measure rotation in spiral galaxies using optical emission lines and are comparable to the most extended H I rotation curves. Despite these large distances, the rotation velocities do not show any sign of falling off in a Keplerian fashion. This forces us to conclude that there must be halos of dark matter in these systems that extend to the limiting radius, or out to $\sim 2.5 R_{25}$ for two of the three S0 disks.

iii) *Shape of Gravitational Potential*

After applying all correction factors to the measured velocities, we find the following ratios between the rotation velocities in the polar rings and the circular velocities in the S0 disks: $V_{\rm ring}/V_{\rm disk} = 0.89 \pm 0.18$ for NGC 4650A, 1.04 ± 0.14 for ESO 415-G26, and 0.98 ± 0.17 for A0136-0801. Therefore, the major result of the present paper is that all three galaxies have

a value of V_{ring}/V_{disk} near 1.0, suggestive of a nearly spherical gravitational potential. The mean ratio for the three galaxies is $\langle V_{ring}/V_{disk}\rangle = 0.97 \pm 0.08$ (rms error of mean derived from the three individual error estimates).

What limits can be put on the shapes of the gravitational potential? Note that in galaxies, equipotentials are generally less flattened than constant-density surfaces. For example, in the extreme case of a completely flat, scale-free disk, equipotential surfaces still have a flattening of $c/a = 0.5$, where a and c are the equatorial and polar dimensions respectively (Monet, Richstone, and Schechter 1981). In the following, our discussion of the shape refers to the gravitational potential, unless stated explicitly otherwise.

To facilitate estimating the shape of the potential from observed velocities, we have recomputed velocities and axial ratios of closed polar orbits in the scale-free gravitational potential of Monet, Richstone, and Schechter (1981). This potential has the form

$$\Phi(R, \theta) = V_{cir}^2 \ln\left(\frac{R}{R_0}\frac{1 + e|\cos\theta|}{1 + e}\right) \quad (5)$$

and represents a cold, flat disk embedded in a nonrotating isothermal halo with an isotropic velocity dispersion. Here, V_{cir} is the circular velocity in the plane of the disk and $e = M_{disk}/(M_{disk} + M_{halo})$ is the fraction of the total mass that is in the disk. The flattening of equipotential surfaces is then

$$\frac{c}{a} = \frac{1}{1 + e}. \quad (6)$$

Consider a Cartesian coordinate system with its origin at the center of the potential, the x- and y-axes in the plane of the disk, and the z-axis perpendicular to it. Let a particle in polar orbit move in the (x, z)-plane. Closed polar orbits can then be computed through simple numerical integration of the equations of motion by starting a test particle at $z = 0$ and any value of x, giving it a vertical initial velocity $V_{vert} \equiv \dot{z}$, and varying this velocity by trial and error until the orbit closes (see Katz and Richstone 1984 for further details). When the orbit closes, a particle reaches its maximum height at the pole ($x = y = 0, z = z_{max}$), moving horizontally with $V_{pol} \equiv \dot{x}$ and, of course, $\dot{z} = 0$.

Table 6 gives the results of our calculations as a function of the flattening c/a of the gravitational potential. Columns (2) and (3) give the fractional mass in the disk M_{disk}/M_{tot} and the ratio of halo mass to disk mass M_{halo}/M_{disk} (where $M_{tot} = M_{disk} + M_{halo}$). Column (4) then gives V_{pol}/V_{equ}, the ratio between the orbital velocity at the pole and the circular velocity in the equator of the disk ($V_{equ} \equiv V_{cir}$); this ratio lends itself for direct comparisons with the ratio V_{ring}/V_{disk} measured in polar-ring galaxies. Column (5) gives V_{vert}/V_{equ}, where V_{vert} is the vertical velocity in closed polar orbit at the crossing of the disk plane. Column (6) gives V_{pol}/V_{vert}. This ratio is more difficult to compare with observations but is included here to compare with Katz and Richstone (1984), who report values of V_{pol}/V_{vert} for their models rather than V_{pol}/V_{equ}.[3] Finally, Column (7) gives z_{max}/x_{max}, the ratio between the vertical and horizontal semiaxes of a closed polar orbit.

To facilitate estimating the shape of equipotentials, the simple linear relation

$$\frac{c}{a} = -0.215 + 1.2117\frac{V_{pol}}{V_{equ}} \quad (7)$$

represents the data of Table 6 to better than 1%, with the exception of the first entry, which is reproduced to 2%.

The flattening of the potential of the three polar-ring galaxies can now be estimated from the values of V_{ring}/V_{disk} given in Table 5. We find $c/a = 0.86 \pm 0.21$ for the equipotentials of NGC 4650A, 1.05 ± 0.17 for ESO 415-G26, and 0.98 ± 0.21 for A0136-0801. Here, we have assumed that to a first approximation equation (7) holds for prolate as well as oblate equipotentials, at least for small deviations from sphericity. The main result, then, is that at radii of $\sim 0.6R_{25}$ the equipotentials of all three systems are nearly spherical. Since the distribution of luminous matter is highly flattened, a nearly spherical dark halo must be the dominant massive component within this radius.

Two limitations to our analysis should be kept in mind. First, our conclusions about the shape of the potential are valid only for radii $\sim 0.6R_{25}$, where polar-ring and disk velocities can be compared. We would guess that at smaller radii the equipotentials tend to be flatter because of the increased influence of the flat and truncated mass distribution of the S0 disks. If the gravitational potential of a polar-ring galaxy were exactly spherical at every radius, there would be no differential

[3] In comparing the data of Table 6 with previous work, note that the ratio V_{pol}/V_{equ} in SWR is the same as V_{pol}/V_{equ} here, whereas the ratio V_{pol}/V_{equ} in Katz and Richstone (1984) would correspond to V_{pol}/V_{vert} here. In other words, we use V_{equ} to designate the circular velocity in the disk, whereas Katz and Richstone use V_{equ} to designate the vertical velocity in the polar orbit at disk crossing.

TABLE 6

POLAR ORBITS IN MODEL POTENTIAL

c/a (1)	M_{disk}/M_{tot} (2)	M_{halo}/M_{disk} (3)	V_{pol}/V_{equ} (4)	V_{vert}/V_{equ} (5)	V_{pol}/V_{vert} (6)	z_{max}/x_{max} (7)
0.50.....	1.00	0.00	0.579	1.667	0.347	1.696
0.55.....	0.82	0.22	0.626	1.582	0.396	1.582
0.60.....	0.67	0.50	0.671	1.504	0.446	1.484
0.65.....	0.54	0.86	0.715	1.430	0.500	1.400
0.70.....	0.43	1.33	0.758	1.360	0.557	1.324
0.75.....	0.33	2.00	0.800	1.294	0.618	1.258
0.80.....	0.25	3.00	0.841	1.230	0.684	1.197
0.85.....	0.18	4.67	0.882	1.169	0.754	1.142
0.90.....	0.11	8.00	0.922	1.111	0.830	1.091
0.95.....	0.05	18.00	0.961	1.055	0.911	1.044
1.00.....	0.00	∞	1.000	1.000	1.000	1.000

NOTE.—Model potential is scale-free gravitational potential by Monet *et al.* 1981.

precession. In this case it would be difficult to understand why the polar rings are generally found to be nearly perpendicular to the inner S0 disks, since any angle would be stable. While angles of 15°–25° from perpendicular are fairly common (Whitmore 1984), polar rings with angles from 30° to 70° are quite rare. Although several candidates can easily be found in Arp (1966), it is our impression that they would be much more prevalent if the potential were spherical at all radii. A detailed study of the probability of identifying these systems at various orientations needs to be made.

A second limitation in our analysis is the assumption that the observed polar rings may be modeled by closed polar orbits passing vertically through the S0 disk. Should this assumption be incorrect, the observed ring velocities would not correspond to the model V_{pol}. In such a case, the velocities along the apparent minor axis of a ring would in general be nonzero. In NGC 4650A, we have been able to check on this prediction by measuring ring velocities from a spectrum taken with the slit at P.A. = 63° or ~10° from the apparent minor axis of the ring in the inner region. Since the slit is not aligned exactly on the minor axis, we expect a slight velocity gradient. We can predict this gradient using the procedure described in Burbidge and Burbidge (1975). Although the warped nature of the polar ring makes the determination uncertain, a typical value of the velocity at 6″ would be 5 ± 4 km s^{-1}, with positive velocities toward the northeast. The observed velocities are slightly larger than our prediction; the average velocity at 6″ is 15 ± 5 km s^{-1} (-9 ± 7 km s^{-1} in the southwest and $+21 \pm 7$ km s^{-1} in the northeast). If real, the difference between the observed and predicted velocities near the minor axis of the polar ring translates to a difference of only 5° from perpendicular. In fact, our values of V_{ring}/V_{disk} imply axis ratios z_{max}/x_{max} of closed polar orbits (Table 6) which are likely to be circular to within $\sim \pm 10\%$ for the three systems studied here.

While the measurements of velocities near the minor axis of NGC 4650A are reassuring, they are for only one polar ring. Another encouraging fact is that radio observations of H I rings in S0 galaxies show a well-ordered velocity field indicative of circular velocities (van Woerden, van Driel, and Schwarz 1983). Similar measurements for several other polar rings are needed to firmly determine the shape of the orbits in these galaxies.

b) *Ages of Polar Rings*

A determination of the ages of polar rings might provide some important clues about how these systems originated. In addition, it may eventually allow us to estimate the frequency of accretion events. Instead of ages, however, only settling times for gaseous rings have been estimated until now, calculated from differential precession rates in a flattened gravitational potential (e.g., Richstone and Potter 1982; Tohline, Simonson, and Caldwell 1982; SWR; SUB). Since decay lifetimes can exceed a Hubble time for nearly spherical potentials, an independent estimate of the true ages of polar rings is desirable. We here attempt such estimates from a combination of spectroscopic and photometric arguments.

Several lines of argument suggest that the ring of NGC 4650A is relatively young. The presence of strong Balmer absorption in the nucleus suggests a burst of star formation within the last $1–2 \times 10^9$ yr, although prolonged infall of gas and star formation from an earlier accretion event cannot be ruled out. The fact that the stellar debris in the outskirts of the galaxy is still clumpy rather than dispersed throughout the halo also suggests that the polar ring could not be more than a few rotation periods old. Since the rotation period at the edge of the ring (15.5 kpc) is 0.8×10^9 yr, this accretion event is unlikely to date back more than $1–3 \times 10^9$ yr. The extremely blue $B-V$ color reported for the outer ring of NGC 4650A using photographic photometry (Sérsic and Agüero 1972) suggests strong ongoing star formation and, presumably, a relatively young age. CCD photometry over a wider spectral range will be required to derive reliable colors and an estimate of the age. The warped and irregular nature of the ring may indicate that the system has not yet had time to settle into a regular disk. This again would presumably require a few orbital periods. All these arguments suggest that an accretion event occurred in NGC 4650A within the last $1–3 \times 10^9$ yr.

The polar ring in ESO 415-G26 also appears to be quite young. The faint shell-like structures in the outer regions give only a weak upper limit to the age, since simulations indicate that these features may persist for 6–10 rotational periods (Schweizer 1983; Quinn 1984; Hernquist and Quinn 1986). The presence of a conspicuous loop on the north side at ~43″ = 19 kpc is probably our best clue (see Fig. 7). This feature is unlikely to be more than a few orbital periods old. If we assume a constant rotational velocity beyond our outermost point, a period of 0.6×10^9 yr and an age for the polar ring of $1–3 \times 10^9$ yr is suggested.

Observations of neutral hydrogen by van Gorkom, Schechter and Kristian (1987) provide more evidence of a young age for the rings in NGC 4650A and ESO 415-G26. They find that polar-ring galaxies are generally rich in H I, and the H I is generally aligned with the ring. ESO 415-G26 is the most prominent exception, with the H I distributed nonsymmetrically and extending well beyond the optical image. NGC 4650A shows similar but less pronounced asymmetries. They suggest that the H I distribution in these two systems indicates there has not been enough time for the gas to settle into the ring and complete its star formation.

The age of A0136-0801 is essentially indeterminate. Although we do not have a CCD image of this galaxy, our best photographic plate of the outer region does not show any tidal debris, suggesting an older age than for NGC 4650A or ESO 415-G26. Another possibility might be that the companion galaxy that merged with the central S0 may have been very gas-rich, so that relatively little stellar debris was dispersed into the halo. The lack of Balmer absorption in the nucleus would be compatible with either explanation (see Whitmore, Rubin, and Ford 1982 for a picture of the spectrum). The regularity of the polar ring suggests that at least several orbital periods have elapsed. This puts a lower limit of at least $2–3 \times 10^9$ yr on the age of the ring. Since the polar ring is more nearly perpendicular than in NGC 4650A or ESO 415-G26 (Whitmore 1984), this system may be more stable against disruption by differential precession, and the true age of the ring of A0136-0801 may be of order 10^{10} yr.

Another polar-ring galaxy for which a reasonable age estimate can be made is NGC 2685, the "Helix" galaxy. The extremely chaotic appearance of the outer helical material suggests that this system is quite young, probably on the order of 1×10^9 yr (Shane 1980).

It was noted in SWR that emission lines in the polar-ring spectra of A0136-0801 extended slightly beyond the inner and outer edges of the ring as observed in the broad-band image. Similarly, the emission on the east side of ESO 415-G26 runs from 10″ to 34″, although the ring appears to be only ~2″ wide

in our CCD frames. This effect is even more prominent in AM 2020-5050 (Schweizer and Whitmore 1986), where the ring is very narrow yet the emission is observed all the way into the nucleus. The existence of S0 galaxies with neutral hydrogen rings but no optical counterpart (e.g., van Woerden, van Driel, and Schwarz 1983; Knapp, van Driel, and van Woerden 1985) is a more extreme example of this phenomenon. It appears that even when the broad-band image shows a narrow ring, the emission lines indicate the presence of a disk. This suggests that star formation primarily occurs within a narrow ring within an extended gas disk. Simonson (1982) has suggested that in a precessing and settling gas disk, there is at any time a narrow region of the most intense cloud collisions. If this mechanism is responsible for the narrow rings, it may be possible to date the ring by modeling the polar-ring galaxies. Another possibility is that an interaction with the S0 disk may produce a ring of recent star formation. The interaction might be similar to the effect a bar has on a disk (Schwarz 1981).

In summary, a series of arguments based on spectroscopy, photometry, and geometry of the rings suggests that the polar rings in NGC 4650A and ESO 415-G26 formed within the last $1–3 \times 10^9$ yr. The helix in NGC 2685 is probably about the same age. The age of the ring of A0136-0801 is indeterminate, but it is surmised to be quite old from the ring's very regular appearance. A better understanding of exactly how the rings evolve may allow us to estimate the age of these systems based on the morphology of the ring.

c) *Origins of Rings*

The galaxies NGC 4650A and ESO 415-G26 offer sufficient clues to justify our making some guesses about the origin of their polar rings. We will not focus on the detailed processes through which polar rings can form around S0 galaxies from accreted foreign material, processes which have been discussed before (e.g., SWR) and for which the presence of luminous debris in the halo (van Gorkom, Schechter, and Kristian 1987; Figs. 3 and 7 here) provides supporting evidence. Rather, the challenge is whether we can identify the likely source of foreign material. Is it the proverbial "small, gas-rich companion" that fell in, as first proposed for NGC 2685 by Toomre (1977) and invoked by many since, or is it perhaps a neighbor galaxy which transferred some material from its outskirts during a close encounter? Both mechanisms, wholesale merging and accretion through mass transfer, seem viable candidates for supplying polar-ring material (SWR; Hernquist and Quinn 1986).

Of the three galaxies discussed in the present paper, NGC 4650A lies the nearest to a potential donor galaxy. It is a member of the Centaurus group (Sérsic and Agüero 1972) and appears at only $5'.7 = 88$ kpc projected distance from NGC 4650, a barried spiral ~ 4 times as large and luminous ($\Delta B \approx 1.5$ mag) as the main body of NGC 4650A itself (see Fig. 9*c* [Pl. 14]). The velocity difference between the two galaxies is only 92 km s^{-1} (heliocentric $V = 2996$ km s^{-1}; Huchra 1983). Therefore, a recent close encounter between the two galaxies with some mass transfer is quite reasonable. Figure 9 shows a sequence of three galaxy pairs that may illustrate configurations before, during, and after mass transfer. To travel the protected separation of 88 kpc with a hypothetical transverse velocity of 100 km s^{-1}, NGC 4650A would need only 0.9×10^9 yr, a time span compatible with the estimated age of $1–3 \times 10^9$ yr for its ring (§ IV*b*). In a group environment a merger, of course, cannot be excluded. Yet note that despite the presence of some luminous shreds in its outskirts, NGC 4650A lacks the extensive asymmetric outer envelope found in ESO 415-G26, or any evidence of ripples. Therefore, the accreted material may have had relatively few old stars per unit gas mass. Such a gas-rich mixture is more typical of the outskirts of spiral galaxies than of whole galaxies. We suggest, then, that the material for the ring of NGC 4650A is likely to have been supplied by NGC 4650 through a mass transfer that occurred a few times 10^9 yr ago, rather than the wholesale merger of a recently consumed galaxy.

The situation seems different for ESO 415-G26. Whereas it has a nice set of ripples and an extensive asymmetric envelope (Fig. 7), it lacks any near neighbor. Although it may be a member of a very loose group (no redshift data available), the nearest galaxy of comparable brightness is an elliptical at a projected distance of $\sim 12' \approx 310$ kpc south, hardly a likely donor of gas. The nearest gas-rich galaxy is an irregular of extremely low surface brightness at $\sim 17' \approx 440$ kpc northwest, a possible gas donor but too poor in old stars to have contributed the observed ripples. The only good candidate donors are two spirals, one at $25' \approx 650$ kpc east and the other at $33' \approx 860$ kpc northeast. The travel times for a hypothetical transverse velocity of 100 km s^{-1} are of order $6–9 \times 10^9$ yr, considerably longer than our estimated age of $1–3 \times 10^9$ yr for the polar ring (§ IV*b*). Therefore, for ESO 415-G26 the odds would seem to be in favor of a wholesale merger, though mass transfer cannot be ruled out. If the strength of the ripples are a guide, we would guess that the intruder was not just a gas-rich dwarf, but actually a spiral galaxy not much smaller than ESO 415-G26 itself.

For A0136-0801 we can make no intelligent guess concerning the source of polar-ring material. Its lack of tidal signatures and presumed old age offer no clues. The nearest potential donor galaxies are two spirals, one at $18'.1 \approx 590$ kpc projected distance northwest and the other at $23'.6 \approx 770$ kpc east-southeast; redshifts are not available. Transverse travel times to each would be of order $5–10 \times 10^9$ yr, certainly compatible with the presumed old age of the ring ($\geq 2–3 \times 10^9$ yr, see § IV*b*). But in the absence of more information, a wholesale merger seems equally possible.

In summary, we suggest that (1) NGC 4650A may have received its polar-ring material through a recent mass transfer from NGC 4650; (2) ESO 415-G26 may have formed its ring from material acquired in a merger with a relatively large, gas-rich galaxy; and (3) A0136-0801 has yielded no clues yet concerning the origin of its ring.

V. SUMMARY

The new observations presented in this paper provide support for the hypothesis that polar rings form by the accretion of material from a companion galaxy either during a close encounter or in a merger. The unusual geometry of these systems provides us with an opportunity to probe the vertical shape of the gravitational potential. The following conclusions are based on observations of the three polar-ring galaxies NGC 4650A, ESO 415-G26, and A0136-0801.

1. The inner components of all three systems have the light distribution and kinematics of S0 disk galaxies.

2. All three galaxies have flat or rising rotation curves and increasing M/L ratios in the outer regions. This indicates the presence of massive dark halos extending well beyond the R_{25} isophote of the S0 components (to $2.6R_{25}$ in the case of A0136-0801).

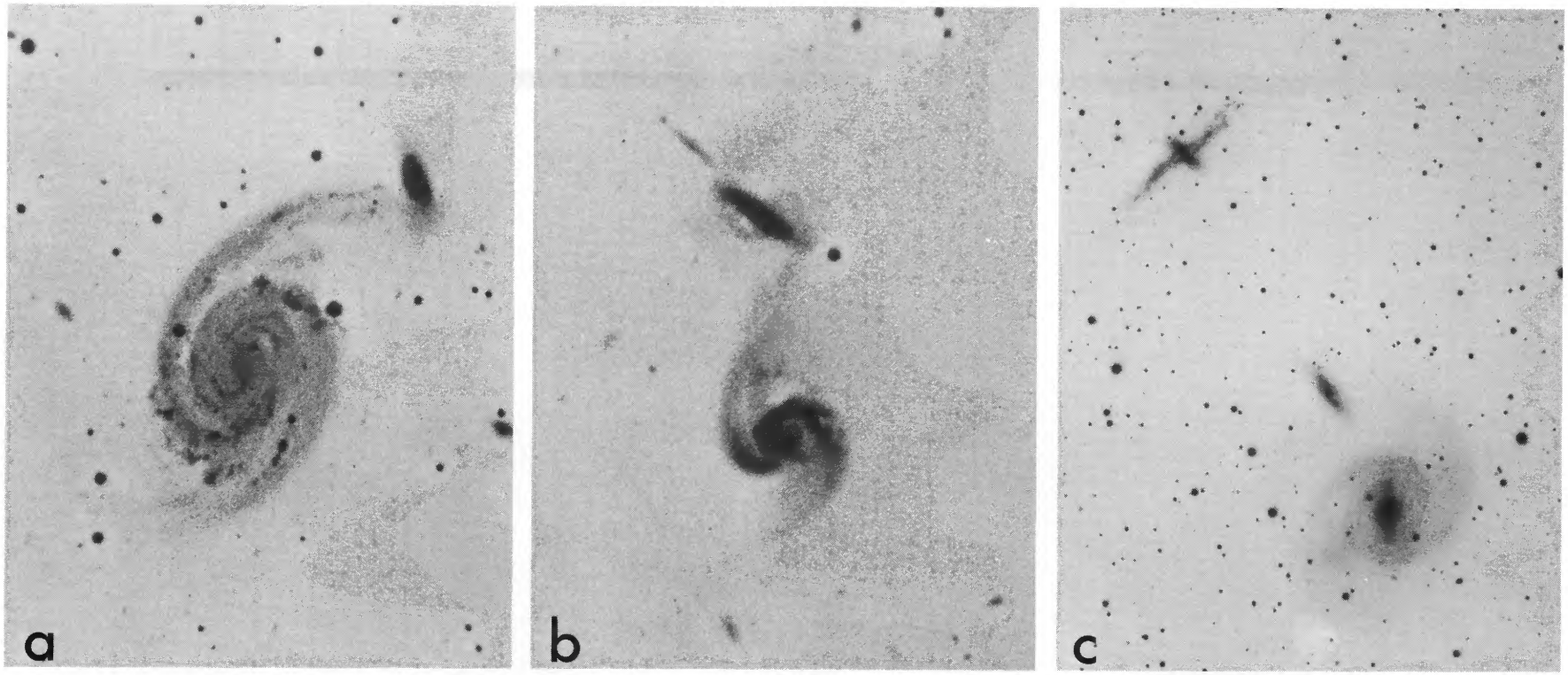

FIG. 9.—Three galaxy pairs illustrating the presumed formation of polar rings through mass transfer. (*a*) NGC 7753 (spiral) and NGC 7752, probably at an early stage of tidal interaction; (*b*) NGC 3608, where luminous matter transferred from the main spiral seems to wrap around an S0 companion; and (*c*) NGC 4650A (*top left*), whose polar ring may have formed out of material transferred from NGC 4650 (barred spiral) during a recent collision. ([*a*] and [*b*] reproduced from Arp 1966.)

WHITMORE, MCELROY, AND SCHWEIZER (*see* page 453)

3. A comparison between rotational velocities in the polar rings and the S0 disk shows they are about the same at equal distances from the center. The mean ratio for the three galaxies is $V_{ring}/V_{disk} = 0.97 \pm 0.08$. From a model with a scale-free potential, we estimate axial ratios of the equipotentials of the three galaxies of $c/a = 0.86 \pm 0.21$, 1.05 ± 0.17, and 0.98 ± 0.20. This provides strong evidence that at distances corresponding to $\sim 0.6R_{25}$ the gravitational potential is nearly spherical since the distribution of luminous matter is highly flattened, a nearly spherical dark halo must be the dominant massive component within this radius.

4. Luminous material suggestive of tidal debris has been detected in the outer regions of NGC 4650A and ESO 415-G26, providing support of the accretion hypothesis for polar-ring formation. The red color of the debris in ESO 415-G26 ($B-V = 0.90 \pm 0.08$), and the blue colors of the rings in all three galaxies, are consistent with a scenario in which the stars of the victim galaxy disperse into the halo while the gas settles into a polar ring that forms new stars.

5. Several lines of argument, including ripples in the luminous debris, presence or absence of warps in the polar rings, the presence of Balmer absorption lines in the S0 disks, the blue colors of the polar rings, and the presence of extended, asymmetric H I, lead us to suggest that the polar rings in NGC 4650A and ESO 415-G26 formed within the last $1-3 \times 10^9$ yr. The age of A0136-0801 is difficult to determine but is surmised to be more than $2-3 \times 10^9$ yr from the absence of visible debris and the ring's regular appearance.

6. Even in cases where the polar-ring material is found in a narrow ring, emission lines are observed over a more extended region, suggesting the presence of a low-luminosity gaseous disk. The optical ring may be the region of this gaseous disk which is undergoing the most intense star formation.

7. The presence of a nearby companion to NGC 4650A (NGC 4650), and the lack of an extensive stellar envelope, lead us to guess that this galaxy received its polar-ring material through a recent mass transfer rather than a wholesale merger. On the other hand, ESO 415-G26 has an extensive stellar envelope and no nearby companion, so a merger of a spiral galaxy of comparable size is likely.

We would like to thank Vera C. Rubin for measuring the emission-line rotation curve for ESO 415-G26, Halton C. Arp for permission to reproduce Arp 86 and 87 from his Atlas, Nelson Caldwell for making the CCD image of NGC 4650A available to us, John Huchra for communicating redshifts in advance of publication, Peter Quinn for several useful discussions, and Marylin Bell for helping with the photometric reductions. F. S. gratefully acknowledges partial support from the National Science Foundation through grant AST 83-18845.

APPENDIX

OBSERVATIONS OF VELOCITY DISPERSION STANDARDS: NGC 488, NGC 628, NGC 1052, AND NGC 7619

Spectroscopic observations of four additional galaxies were made to test the reliability of our reduction procedures. The data for these galaxies are presented in Table 7 and Figures 10–13. All four galaxies are listed as central velocity dispersion standards by

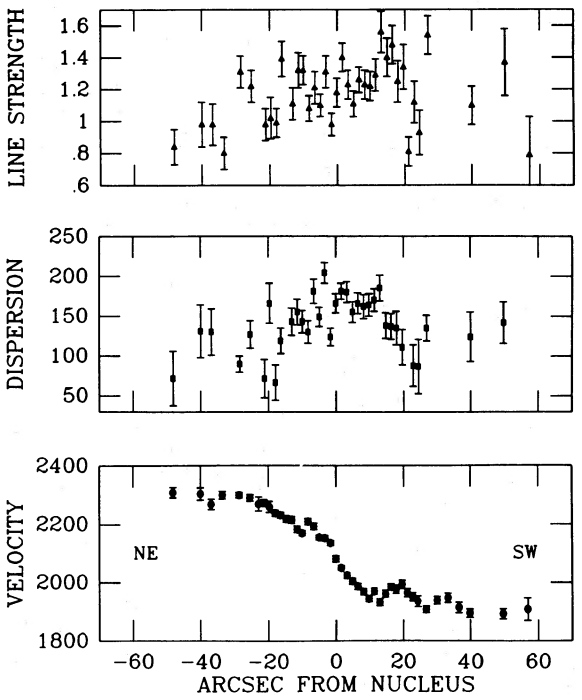

FIG. 10

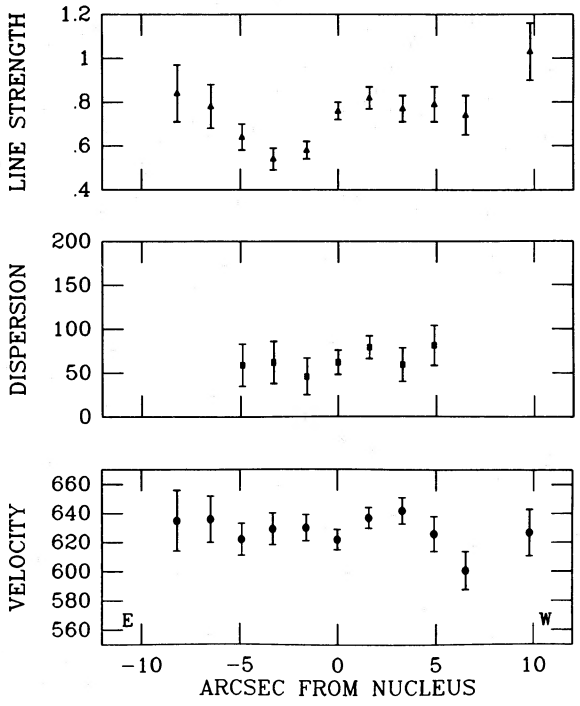

FIG. 11

FIG. 10.—Line strength index, rotational velocity, and velocity dispersion along the major axis of NGC 488
FIG. 11.—Same as Fig. 10, for NGC 628

TABLE 7

STELLAR VELOCITIES IN THE STANDARD GALAXIES

R	cz (km s^{-1})	σ (km s^{-1})
N 488 (P.A. = 8°; northeast to southwest)		
−48″.1	2309 ± 18	72 ± 34
−39.9	2304 ± 21	131 ± 33
−36.7	2268 ± 18	130 ± 29
−33.4	2299 ± 13	...
−28.5	2299 ± 9	90 ± 10
−25.3	2290 ± 11	127 ± 17
−22.8	2269 ± 24	...
−21.2	2273 ± 12	72 ± 24
−19.6	2259 ± 19	166 ± 25
−17.9	2238 ± 11	67 ± 22
−16.3	2231 ± 10	119 ± 16
−14.7	2218 ± 11	...
−13.0	2215 ± 12	143 ± 17
−11.4	2183 ± 11	155 ± 16
−9.9	2170 ± 9	143 ± 14
−8.2	2209 ± 10	130 ± 14
−6.5	2193 ± 11	181 ± 15
−4.9	2155 ± 8	149 ± 12
−3.3	2153 ± 10	204 ± 13
−1.6	2136 ± 8	124 ± 11
0.0	2082 ± 10	166 ± 12
+1.6	2051 ± 8	181 ± 10
+3.3	2025 ± 10	180 ± 13
+4.9	2005 ± 10	155 ± 13
+6.5	1987 ± 10	166 ± 13
+8.2	1969 ± 11	162 ± 15
+9.8	1944 ± 10	164 ± 14
+11.4	1970 ± 11	170 ± 14
+13.0	1932 ± 12	185 ± 16
+14.7	1961 ± 12	138 ± 16
+16.3	1984 ± 11	137 ± 16
+17.9	1976 ± 14	135 ± 21
+19.6	1993 ± 14	111 ± 22
+21.2	1964 ± 14	...
+22.8	1950 ± 14	88 ± 26
+24.4	1935 ± 18	87 ± 34
+26.9	1907 ± 11	135 ± 16
+30.2	1938 ± 13	...
+33.4	1946 ± 16	...
+36.7	1913 ± 18	...
+39.9	1894 ± 14	124 ± 31
+49.7	1892 ± 17	142 ± 26
+57.0	1908 ± 38	...
NGC 628 (P.A. = 90°; west to east)		
−8″.2	635 ± 21	...
−6.5	636 ± 16	...
−4.9	622 ± 11	59 ± 24
−3.3	629 ± 11	62 ± 24
−1.6	630 ± 9	46 ± 21
0.0	622 ± 7	62 ± 14
+1.6	637 ± 7	79 ± 13
+3.3	642 ± 9	59 ± 19
+4.9	626 ± 12	81 ± 23
+6.5	601 ± 13	...
+9.8	627 ± 16	...
NGC 1052 (P.A. = 120°; southeast to northwest)		
−21″.2	1536 ± 38	...
−18.7	1499 ± 27	...
−15.5	1496 ± 20	156 ± 39
−13.0	1530 ± 16	...
−11.4	1532 ± 20	166 ± 29
−9.8	1538 ± 36	...
−8.2	1535 ± 31	...
−6.5	1527 ± 18	208 ± 23
−4.9	1503 ± 11	154 ± 17
−3.3	1472 ± 12	230 ± 15
−1.6	1458 ± 10	223 ± 13
0.0	1380 ± 12	254 ± 14
+1.6	1314 ± 11	216 ± 15
+3.3	1304 ± 11	207 ± 14
+4.9	1314 ± 14	160 ± 19
+6.5	1349 ± 14	139 ± 20
+8.2	1340 ± 16	153 ± 24
+9.8	1281 ± 23	162 ± 32
+11.4	1304 ± 27	161 ± 38
+13.0	1299 ± 27	150 ± 39
+14.7	1352 ± 31	166 ± 44
+17.1	1335 ± 24	179 ± 32
+20.4	1324 ± 32	...
NGC 7619 (P.A. = 30°; northeast to southwest)		
−12″.2	3568 ± 30	157 ± 41
−9.8	3494 ± 38	137 ± 55
−6.5	3428 ± 34	191 ± 45
−4.9	3528 ± 33	229 ± 41
−3.3	3599 ± 23	180 ± 30
−1.6	3563 ± 22	228 ± 26
0.0	3655 ± 24	267 ± 27
+1.6	3729 ± 27	231 ± 31
+3.3	3678 ± 28	245 ± 33
+4.9	3645 ± 36	172 ± 49
+6.5	3730 ± 39	180 ± 50
+8.2	3738 ± 24	185 ± 31
+10.6	3691 ± 31	172 ± 41

Whitmore, McElroy, and Tonry (1985). In addition, velocity profiles are available for NGC 1052 and NGC 7619 (Schechter and Gunn 1979; Davies and Illingworth 1986). Previous velocity dispersion measurements of the polar-ring galaxy NGC 4650A have been published by SUB. We find that while our lower values of the velocity dispersion are in good agreement with published values (both NGC 628 and NGC 4650A are within 3 km s^{-1} of previous measurements), our higher values of velocity dispersion are lower than previous measurements by an average of ~20%. We have not made any corrections to the measurements in this paper, since they are for low-dispersion systems.

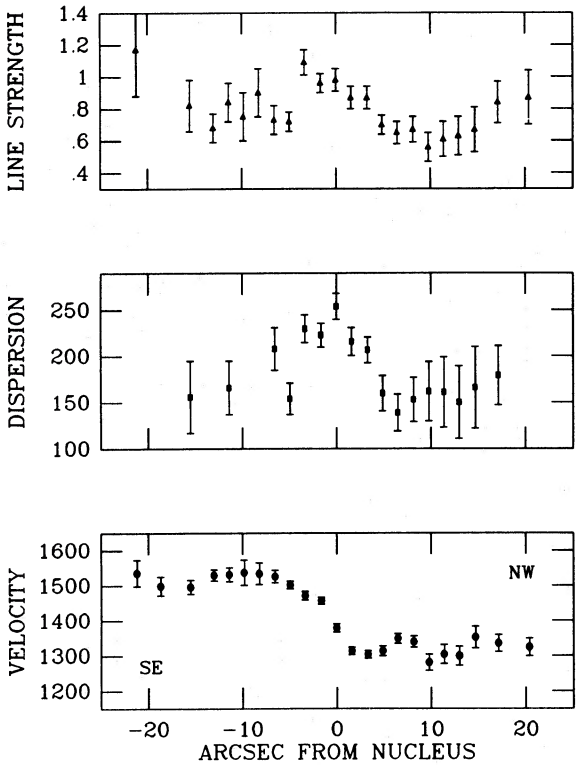

FIG. 12.—Same as Fig. 10, for NGC 1052

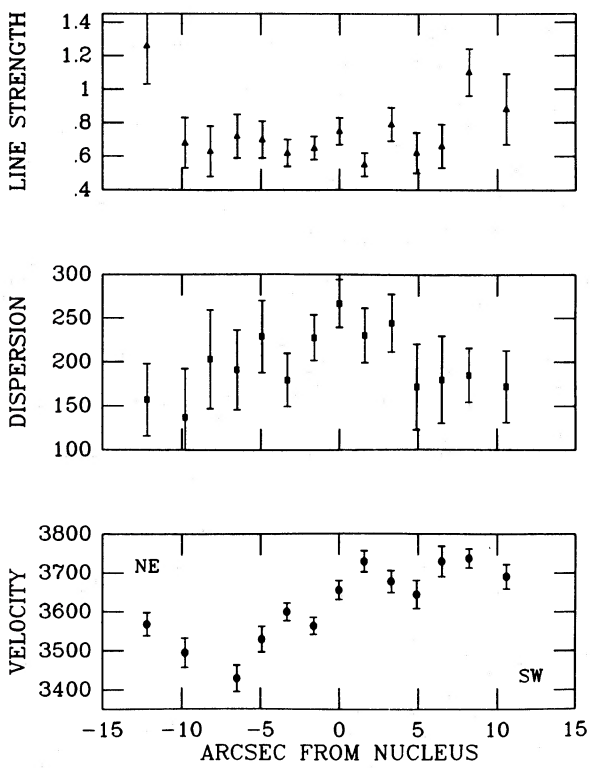

FIG. 13.—Same as Fig. 10, for NGC 7619

REFERENCES

Arp, H. C. 1966, *Atlas of Peculiar Galaxies* (Pasadena: Caltech).
Arp, H. C., and Madore, B. 1986, *A Catalogue of Southern Peculiar Galaxies*, in press.
Athanassoula, E., and Bosma, A. 1985, *Ann. Rev. Astr. Ap.*, **23**, 147.
Boroson, T. 1981, *Ap. J. Suppl.*, **46**, 177.
Burbidge, E. M., and Burbidge, G. R. 1975, in *Stars and Stellar Systems*, Vol. **9**, *Galaxies and the Universe*, ed. A. Sandage, M. Sandage, and J. Kristian (Chicago: University of Chicago Press), p. 101.
Burstein, D., and Heiles, C. 1985, *A.J.*, **87**, 1165.
Davies, R. L., and Illingworth, G. D. 1986, *Ap. J.*, **302**, 2, 234.
de Vaucouleurs, G., and Pence, W. D. 1978, *A.J.*, **83**, 1163.
Frenk, C. S., and White, S. D. M. 1980, *M.N.R.A.S.*, **193**, 295.
Graham, J. 1982, *Pub. A.S.P.*, **94**, 244.
Heidmann, J., Heidmann, N., and de Vaucouleurs, G. 1971, *Mem. R.A.S.*, **75**, 85.
Hernquist, L., and Quinn, P. J. 1987, *Ap. J.*, **312**, 1.
Illingworth, G., and Schechter, P. L. 1982, *Ap. J.*, **256**, 481.
Jahreiss, H., and Wielen, R. 1983, in *IAU Colloquium 76, The Nearby Stars and the Stellar Luminosity Function*, ed A. G. Davis Philip and A. R. Upgren (Schenectady: Davis), p. 277.
Katz, N., and Richstone, D. O. 1984, *A.J.*, **89**, 975.
Knapp, G. R., van Driel, W., and van Woerden, H. 1985, *Astr. Ap.*, **142**, 1.
Kuzmin, G. G. 1956, *Astr. Zh.*, **33**, 27.
Lake, G., and Norman, C. 1983, *Ap. J.*, **270**, 51.
Laustsen, S., and West, R. M. 1980, *J. Ap. Astr.*, **1**, 177.
Monet, D. G., Richstone, D. O., and Schechter, P. L. 1981, *Ap. J.*, **245**, 454.
Oort, J. H. 1965, in *Stars and Stellar Systems*, Vol. **5**, *Galactic Structure*, ed. A. Blaauw and M. Schmidt (Chicago: University of Chicago Press), p. 455.
Quinn, P. J. 1984, *Ap. J.*, **279**, 596.
Richstone, D. O., and Potter, M. D. 1982, *Nature*, **298**, 728.
Rubin, V. C., Ford, W. K., and Thonnard, N. 1980, *Ap. J.*, **238**, 471.
Sargent, W. L. W., Schechter, P. L., Boksenberg, A., and Shortridge, K. 1977, *Ap. J.*, **212**, 326.
Schechter, P. L., and Gunn, J. E. 1978, *A.J.*, **83**, 1360.
Schechter, P. L., and Gunn, J. E. 1979, *Ap. J.*, **229**, 472.
Schechter, P. L., and Kristian, J. 1984, *Carnegie Yrb.*, **83**, 52.
Schechter, P. L., Ulrich, M., and Boksenberg, A. 1984, *Ap. J.*, **277**, 526 (SUB).
Schweizer, F. 1983, in *IAU Symposium 100, Internal Kinematics and Dynamics of Galaxies*, ed. E. Athanassoula (Dordrecht: Reidel), p. 319.
Schweizer, F., Rubin, B. C., and Whitmore, B. C. 1983, *Carnegie Yrb.*, **82**, 581.
Schweizer, F., and Whitmore, B. C. 1986, in preparation.
Schweizer, F., Whitmore, B. C., and Rubin, V. C. 1983, *A.J.* **88**, 909 (SWR).
Schwarz, M. P. 1981, *Ap. J.*, **247**, 77.
Sérsic, J. L. 1967, *Z. Ap.*, **67**, 306.
Sérsic, J. L., and Agüero, E. L. 1972, *Ap. Space Sci.*, **19**, 387.
Shane, W. W. 1980, *Astr. Ap.*, **82**, 314.
Simonson, G. 1982, Ph.D. thesis, Yale University.
Steiman-Cameron, T. Y., and Durisen, R. H. 1982, *Ap. J. (Letters)*, **263**, L51.
Tohline, J. E., Simonsen, G. F., and Caldwell, N. 1982, *Ap. J.*, **252**, 92.
Toomre, A. 1977, in *The Evolution of Galaxies and Stellar Populations*, ed. B. M. Tinsley and R. B. Larson (New Haven: Yale University Observatory), p. 418.
Tsikoudi, V. 1979, *Ap. J.*, **234**, 842.
Tubbs, A. D., and Sanders, R. H. 1979, *Ap. J.*, **230**, 736.
Ulrich, M. H. 1975, *Pub. A.S.P.*, **87**, 965.
van der Kruit, P. C., and Freeman, K. C. 1986, *Ap. J.*, **303**, 556.
van Gorkom, J., Schechter, P. L., and Kristian, J. 1987, *Ap. J.*, **314**, 457.
van Woerden, H., van Driel, W., and Schwarz, U. J. 1983, in *IAU Symposium 100, Internal Kinematics and Dynamics of Galaxies*, ed. E. Athanassoula (Dordrecht: Reidel), p. 99.
Whitmore, B. C. 1984, *A.J.*, **89**, 618.
Whitmore, B. C., and Kirshner, R. P. 1981, *Ap. J.*, **250**, 43.
———. 1982, *A.J.*, **87**, 500.
Whitmore, B. C., Kirshner, R. P., and Schechter, P. L. 1979, *Ap. J.*, **234**, 68.
Whitmore, B. C., McElroy, D., and Tonry, J. 1985, *Ap. J. Suppl.*, **59**, 1.
Whitmore, B. C., Rubin, V. C., and Ford, W. K. 1982, *Carnegie Yrb.*, **81**, 573.
Young, P., Sargent, W. L. W., Boksenberg, A., Lynds, C. R., and Hartwick, F. D. A. 1978, *Ap. J.*, **222**, 450.

DOUGLAS B. MCELROY and BRADLEY C. WHITMORE: Space Telescope Science Institute, 3700 San Martin Drive, Baltimore, MD 21218

FRANÇOIS SCHWEIZER: Department of Terrestrial Magnetism, Carnegie Institution of Washington, 5241 Broad Branch Road N.W., Washington, DC 20015